Neptune's Rings, 1983–1989: Ground-Based Stellar Occultation Observations

I. Ring-like Arc Detections

BRUNO SICARDY,*·† FRANÇOISE ROQUES,† AND ANDRÉ BRAHIC*·†

*Université Paris VII, 2 place Jussieu, 75005 Paris, and †Observatoire de Paris, 92195 Meudon Cédex Principal, France

A systematic campaign of stellar occultation observations by Neptune was conducted by our group between 1983 and 1989, and led to the initial discovery of Neptune's rings. These observations provide 24 independent scans across Neptune's equatorial plane. Two of them give evidence for ring-like arcs around the planet. The two detections, made respectively on July 22, 1984 and August 20, 1985, are the only ones ever observed simultaneously by two or more telescopes. The corresponding lightcurves are analyzed using Neptune's pole position recently determined after the Voyager 2 spacecraft observations. Assuming that the arcs lie in Neptune's equatorial plane, the 1984 detection corresponds to material orbiting 65,300 ± 3000 km from the center of the planet, and the 1985 detection corresponds to material which lies at 63,160 ± 200 km, so that both events are compatible with the Voyager 2 observations of the three arc structures observed near the 63,000-km radius (we propose the names Liberty, Equality, and Fraternity for these arcs). The arc detected in 1984 has a radial width of W_r = 15.1 ± 0.1 km, an azimuthal extension greater than 100 km, and a normal optical depth of 0.074 ± 0.003 (these quantities are projected in Neptune's equatorial plane). The arc detected in 1985 has a radial width of W_r = 15.3 ± 0.2 km and a normal optical depth of 0.058 ± 0.001. Our observations do not show evidence for any additional ring-like arc, nor for any perceptible diffuse, narrow, or broad rings with normal optical depth larger than about 4×10^{-3} near the 63,000- and 53,000-km radii, where the Voyager 2 spacecraft observed continuous Neptunian rings. Finally, a preliminary search on our best lightcurves near these two radii does not show any short, correlated event with equivalent width larger than ~75 m. © 1991 Academic Press, Inc.

1. INTRODUCTION

Neptune's ring and arc discovery is the result of a systematic campaign of ground-based stellar occultation observations and of a remarkable complementarity between ground-based and space research.

In this paper, we report and analyze 24 independent occultation cuts in Neptune's equatorial plane, obtained by our group between 1983 and 1989. Two of these cuts led to the discovery of Neptune's arcs, and are analyzed in this paper using the Neptune pole position recently determined by the Voyager 2 spacecraft observations (Smith et al. 1989). A more complete analysis of all our observations and the estimate of an upper limit for faint material around Neptune will be given in a subsequent paper (paper II). Stellar occultations by the Neptunian rings give very different results when compared to stellar occultations by Uranus' rings. In the latter case, the observations always lead to the detection of the Uranian rings. In the former case, however, most of the observations do not lead to the detection of faint material around Neptune, and only a few observations lead to "positive" detections. This paper is devoted mainly to our positive ground-based detections. "Negative" detections are far from being useless since they bring important observational constraints and physical information (like the arc stability), and they are studied in paper II.

Before 1977, Saturn was still the only planet known to be surrounded by rings. In less than 10 years, the topic of planetary rings was completely renewed, on one hand by the observations at high resolution of Saturn's rings by the Voyager spacecraft, in 1980 and 1981, and on the other hand by the discoveries of ring systems around all of the other giant planets, Jupiter, Uranus, and Neptune. The great variety of physical processes thus unveiled has triggered recent interest in this area, with many new dynamical problems linked to disk evolution and to the formation of the solar system. It is important to note, for these kinds of discoveries, the deep complementarity between ground-based and space observations.

The tenuous Jovian rings were first detected by the Voyager 1 spacecraft (Owen et al. 1979), then imaged by the Voyager 2 spacecraft (Smith et al. 1979), and detected from the Earth (Jewitt et al. 1981).

Narrow rings around Uranus were detected by ground-

based observations of a stellar occultation on March 20, 1977 (Bhattacharyya and Kuppuswamy 1977, Elliot *et al.* 1977a, Millis *et al.* 1977). Later, additional rings were discovered and subsequent observations gave a much better accuracy on ring orbits and physical properties (French *et al.* 1986a). The accuracy on the orbits (a few hundreds of meters) shows the power of ground-based observations, and has allowed us to raise several interesting dynamical problems (French *et al.* 1986b). Complementary results have been provided by the Voyager 2 spacecraft during its encounter with the planet in January 1986 (Smith *et al.* 1986, Lane *et al.* 1986, Tyler *et al.* 1986, French *et al.* 1988).

Without the ground-based detection of Neptune's arcs, the Voyager 2 spacecraft would not have been programmed on time to observe the Neptunian ring system under good conditions during its flyby of the planet in August 1989. As opposed to the 1979 Jupiter encounter, there is unfortunately no second spacecraft scheduled to meet Neptune in the near future.

The search for Neptune's rings has been a controversial subject and has led to several misinterpretations. Details on the history of the Neptunian rings' discovery can be found elsewhere (Brahic 1982, 1985, Hubbard *et al.* 1986, Brahic and Hubbard 1989, Sicardy and Brahic 1989). It is interesting to note that Guinan and colleagues claimed, after the discovery of Uranus' rings, that they had observed a dip in the occultation lightcurve of April 7, 1968 (Guinan *et al.* 1982, Waldrop 1982). The data were never published and most astronomers considered the dip to be spurious. After bright star occultations observed under good conditions in 1981 by several teams around the Pacific Ocean, no clear evidence for light interruption by rings or moons was found, and a paper entitled "no evidence for rings around Neptune" was published (Elliot *et al.* 1981). Reitsema and Hubbard noticed a well-correlated signal interruption while observing on May 24, 1981 from two telescopes, 6 km apart in Arizona (Reitsema *et al.* 1982, Hubbard 1986). Observers hundreds and thousands of kilometers north saw nothing. It seems now that the correlated dips correspond to the stellar occultation by the newly discovered satellite 1989N2 (Smith *et al.* 1989). The first clear evidence for interrupted ring-like material, or "arcs," around Neptune came from a stellar occultation observed in July 1984, in Chile, by a group from the University of Arizona and by our group from Paris Observatory (Roques *et al.* 1984, Brahic 1985, Sicardy *et al.* 1985, Hubbard *et al.* 1986, Brahic *et al.* 1986, 1990). One of the more striking consequences of the Neptunian ring discovery is the diversity of ring systems around the giant planets in the solar system. One can wonder now how many kinds of different ring systems surround other giant planets in the universe.

The 1984 and 1985 observations were, however, a part

of a more systematic observational campaign, started in the early 1980s and leading up to the Voyager encounter in 1989. In the meantime, an exhaustive and continuing analysis of the occultation observations that our group has conducted has not yet been published. The aim of this paper is thus to present this analysis for our data set completed between 1983 and 1989. This study is not complete yet, but should be at least sufficiently detailed and homogeneous to serve as a basis for future comparisons, especially with the Voyager 2 data set, and to stimulate theoretical interpretations.

One of the main difficulties encountered when analyzing these stellar occultations by Neptune and by other planets is the occurrence of frequent "isolated events" in the lightcurves, that is, brief drops of the stellar flux observed by only one telescope, on only one side of the planet. These are to be contrasted with events systematically observed on both sides of the planet, which are the signature of complete rings surrounding the central body. Isolated events are regularly observed in addition to the planetary occultations, and most of them are easily interpreted as artifacts caused by electronic discharges, tracking errors, clouds, or seeing problems. Nevertheless, a few of them remain indistinguishable from real events, i.e., events caused by circumplanetary material (Sicardy *et al.* 1982, 1986). Smoothing effects due to diffraction and the finite size of the stars (projected at the distance of Neptune) are such that real events should be well correlated over a distance of a few kilometers when observed from the ground. This is not in general the case for artifacts.

Thus we propose some definitions: A *secondary* (or *isolated*) event is considered as *real* (i.e., due to circumplanetary material), *not necessarily when it is observed on both sides of the planet from one telescope, but rather when it is observed simultaneously by more than one telescope during the same occultation, or when it is detected at the same radius during different occultations.* The first criterion is of course much stricter and allows one to speak of *confirmed events*, and this strategy, based on the duplication of the observation of a given occultation from different sites, has permitted us to confirm the reality of some of these isolated events, and thus has led to the discovery of arcs around Neptune. Note that the second criterion supposes that the material has a circular orbit in the equatorial plane of the planet. We propose also to define an *arc* as an azimuthally confined object, the word *ring* implying continuity. Then Voyager 2 has observed three coorbital arc structures superimposed on a diffuse ring, near the 63,000-km radius.

In this paper, we analyze the arc detections and make a preliminary search for other detections (with the 1983–1989 observations). We successively present (1) the positive ring detections, i.e., the analysis of the July 22, 1984 and August 20, 1985 events (as a comparison, we

also analyze two events observed on June 22, 1987 with only one telescope), and (2) a set of transformed lightcurves deduced from the 24 scans that our observations provided between 1983 and 1989 (These reduced data show that the two positive detections are the only ones well above the noise, and also above other possible candidates).

In paper II, we give a more complete presentation of these scans of all the observations, including information on the conditions of observations and on the quality of the data (noise, presence of spurious events, etc.). We also give in paper II the physical constraints derived from the negative results, and we search for upper limits on faint material around Neptune from ground-based observations.

General information on the observations, including geographical details, filters and receptors, prediction efforts, and quality of the lightcurves, is provided in Section 2. Brief comments on each observation, as well as the derived reconstructed occultation geometries, are presented in Section 3. The methods of reduction are described in Section 4. In Section 5, the two arc detections are studied in detail. We present also in Section 5 two isolated events observed in June 1987. The other reduced lightcurves are analyzed in Section 6, and an approximate upper limit for continuous, narrow Neptunian rings is estimated. A preliminary comparison with other ground-based and the Voyager observations, as well as some concluding remarks, is provided in Section 7.

2. THE OBSERVATIONS

2.1. General Conditions

During the last decade, the path of Neptune has been crossing the Milky Way, in the region of the Galactic Center (constellation of Sagittarius). This results in a significant increase in stellar occultation frequency. Furthermore, the advent of fast infrared photometry has permitted the observation of more and more numerous candidates. The use of absorbing methane bands at 0.89 and 2.2 μm suppresses the light from the disk of the planet, while not affecting the star brightness, thus leading to high-contrast stellar occultations. The combination of prediction efforts, rapidly circulated information, and appropriate filters yields typically three to five usable stellar occultations by Neptune per year and per site, i.e., occultations for which the flux from the star is a significant fraction of the flux from Neptune.

In total, we have attempted observation of 16 occultations by Neptune, which represents 24 telescope allocations, since some occultations were observed simultaneously from several telescopes. All these attempts are summarized in Table I, which also provides some basic

information about each observation. Geographical details on the observatories are provided in Table II. Note that we have also added in the present list the August 20, 1985 observation made at the Cerro Tololo Inter-American Observatory (CTIO). Of these 25 experiments, 16 were successful, the rest being obliterated by bad weather, faintness of the star, and/or technical failures. Finally, as will be seen from the astrometric reconstructions, these 16 observations yield 24 independent scans in Neptune's equatorial plane, since some of these occultations yield a scan on each side of the planet (Section 3.2). General information about each of these observations is provided in Table I, and the locations of the observatories are given in Table II.

As will be analyzed in paper II, the eventual quality of each occultation lightcurve depends on numerous parameters, three of which are essential: (i) star brightness; (ii) size of the telescope; (iii) quality of the site, plus the elevation of the star in the sky, the relative velocity of Neptune in the sky plane, the proximity of twilight, etc. Note that because of the low declination of Neptune in the sky ($\sim -22°$), the European Southern Observatory (ESO, Chile, latitude $\sim -29°$) is particularly well located for this kind of observation. At the Canada–France–Hawaii Telescope (CFHT, Hawaii), Neptune culminates at about 59° above the horizon, while at Pic du Midi Observatory (OPMT, France) and Haute Provence Observatory (OHP, France), it culminates at only 26°.

The low elevation of Neptune, the faintness of the star, or the mere presence of clouds prevented the recording of data on October 22, 1985, May 4, 1986, August 23, 1986, and July 30, 1988. Finally, part or all of certain observations were spoiled by purely technical problems. This includes breakdown in the acquisition software (August 25, 1988, July 7/8, 1989), failure of the chopping mirror control (July 9, 1987), and the presence of too many electrostatic discharges on the detector (July 25, 1988).

2.2. Detectors

The observations were made with two kinds of high-speed photometer: (i) an arsenium–gallium (AsGa) photometer and a Quantacon photometer at ~ 0.9 μm and (ii) indium–antimonide (InSb) photometers at ~ 2.2 μm.

The AsGa photometer, used at Pic du Midi for the September 12, 1988 and July 7/8, 1989 observations, has two channels, one used in the 0.89-μm methane band and the other at 0.75 μm. The first channel is essentially sensitive to the stellar flux, while the second channel essentially records the flux from Neptune, thus monitoring sky transparency, seeing effects, and, more generally, acquisition problems. This discriminates real events (due

TABLE I
Conditions of Observation

Date	Observatory and telescope	Wavelength (μm)[b]	Integration time (sec)	Star magn.	Star veloc. (km/s)	B[a]	P[a]
June 15, 1983	CFH 3.6-m	2.18	0.3	6.9	24.2	-18°49'54"	23°44'53"
July 22, 1984	ESO 1-m	2.18	0.01	4.2	20.1	-18°15'40"	22°49'00"
"	ESO 50-cm	0.81	0.01	6.6	"	"	"
August 20, 1985	ESO 1-m	2.18	0.01	6.4	11.1	-19°50'38"	21°32'18"
"	CFH 3.6-m	2.18	0.01	"	"	"	"
"	CTIO 1.5-m	2.18	0.01	"	"	"	"
October 22, 1985	ESO 1-m			no data			
April 23, 1986	CFH 3.6-m	2.18	0.05	12.4	8.2	-21°31'14"	17°54'54"
May 4, 1986	ESO 1-m			no data			
August 4, 1986	OPMT 2-m			no data			
August 23, 1986	CFH 3.6-m			no data			
June 22, 1987	ESO 3.6-m	2.18	0.01	10.1	24.1	-21°50'23"	17°05'02"
July 9, 1987	CFH 3.6-m			no data			
July 25, 1988	ESO 3.6-m			no data			
"	ESO 1-m			no data			
July 30, 1988	ESO 2.2-m			no data			
"	ESO 1-m			no data			
August 2, 1988	ESO 2.2-m	2.18	0.03	10.5	19.9	-22°10'11"	16°08'53"
"	ESO 1-m	2.18	0.03	"	"	"	"
August 25, 1988	CFH 3.6-m	2.18	0.02	10.3	11.7	-22°05'17"	18°28'02"
September 12, 1988	OPMT 2-m	0.88	0.1	11.4	3.2	-21°57'33"	16°35'03"
"	OHP 1.93-m	2.18	0.066	6.8	"	"	"
July 7, 1989	ESO 2.2-m	2.18	0.01	5.5	23.8	-23°03'25"	13°50'40"
July 7, 1989	ESO 1-m	2.18	0.01	"	"	"	"
July 7, 1989	OPMT 2-m	0.88	0.05	7	"	"	"

[a] B is the Neptunocentric elevation of the Earth and P is the position angle of Neptune's pole in the plane of the sky, counted counterclockwise from the north. The assumed Neptune pole direction is α_N = 298.9° and δ_N = 42.8° (1950).

[b] The photometers are Insb at 2.18 μm, Quantacon at 0.81 μm,and AsGa at 0.88 μm.

to rings for instance) from spurious dips associated with ground or atmospheric problems. The one-channel Quantacon photometer, used for the July 22, 1984 observation on the ESO 0.5-m telescope, was used in chopping mode. All the rest of the observations made use of InSb photometers, also in chopping mode, except for the August 20, 1985 observations at CFHT, for which the *direct* signal was recorded. This choice was made to decrease

TABLE II
Locations of the Observatories[a]

Site	CFHT	ESO	CTIO	OPMT	OHP
Latitude	19°49'41".9	-29°15'21".0	30°09'56".3	42°56'12"	43°55'45".6
Longitude	155°28'18".0 W	70°43'53".7 W	70°48'54".5 W	00°08'32" E	05°42'50" E
Altitude (m)	4200	2350	2225	2860	650

[a] CFHT, Canada France Hawaii Telescope; ESO, European Southern Observatory; CTIO, Cerro Tololo Inter-American Observatory; OPMT, Observatoire du Pic du Midi de Toulouse; OHP, Observatoire de Haute Provence.

the overall time constant and thus to increase the spatial resolution. This technique is fruitful only with very bright stars, for which the sky and Neptune contributions are negligible.

2.3. Prediction

The occultation predictions were taken from two main sources. A first survey was made on yellow photographic plates (Mink *et al.* 1981, Mink and Klemola 1985), and yielded the star candidates for the occultations of June 15, 1983, July 22, 1984, April 23, 1986, August 2, 1988, September 12, 1988, and July 7/8, 1989. A more recent survey is based on R and I plates (Nicholson, private communication, and Nicholson *et al.* 1988), and allowed us to observe the occultations of August 20, 1985, June 22, 1987, and August 25, 1988. Further information on the photometry of the candidate stars is provided by Covault and French (1986). It should be noted that the use of plates taken in the red has dramatically increased the number of candidate stars. Actually, direct infrared surveys using array detectors at 2.2 μm would be now most useful for predicting forthcoming occultations by Neptune and the other giant planets.

3. DATA

Before examining in more detail the results connected to the Neptunian arcs and rings, we first give in this section a general description of the raw data. We also present the reconstructed geometries of these occultations, i.e., the paths of the stars relative to Neptune, in the plane of the sky.

3.1. The Observations

3.1.1. June 15, 1983. This occultation (N30 in Mink *et al.* 1981) was observed under excellent atmospheric conditions from Hawaii (CFHT). The resulting lightcurve is one of the least noisy of all, in spite of the modest elevation of the star above the horizon: 28° at the beginning of the observation and 15° at the end. Because of the particular geometry of the event, the star scanned the equatorial plane of Neptune down to 28,000 km, i.e., only 1.1 planetary radii (Fig. 1b). This circumstance, combined with the high signal-to-noise ratio, makes this scan the most complete to date in our set. In particular, this observation showed that Neptune does not possess continuous diffuse rings with normal optical depth larger than 6×10^{-3}, nor narrow opaque rings wider than 300 m (Sicardy *et al.* 1986). These limits are discussed again and improved, when we include the more recent observations (see Section 6).

3.1.2. July 22, 1984. The very bright star (SAO186001, or N34 of Mink *et al.* 1981) led to the first unambiguous detection of ring-like material around Neptune (Roques *et al.* 1984, Sicardy *et al.* 1985, Hubbard *et al.* 1986, Brahic *et al.* 1986; and see Section 5). It was observed simultaneously from ESO (1-m and 50-cm telescopes) and from the CTIO 0.9-m telescope, about 100 km away from ESO. The corresponding lightcurves have quality comparable to that of the June 15, 1983 observation. The star missed the planet by a few hundreds of kilometers, as projected in the plane of the sky (Fig. 1a and see the discussion below), so that there was no occultation, but only an appulse. The closest approach to the planet's limb occurred around 51,000 km in the equatorial plane, and one can note the simultaneous detection, around 65,000 km, of the arc event on both telescopes (Fig. 5a). A first report of this arc discovery, including the CTIO data, is presented in Hubbard *et al.* (1986). We present here a more precise discussion on the geometrical and optical properties of this arc, taking into account the recent Neptune pole position determined after the Voyager 2 flyby (Section 5). Also, we estimate in Section 6 the upper limit for the material density when the star recrossed the arc's orbit.

3.1.3. August 20, 1985. This very bright candidate star (discovered by Nicholson, Matthews, and Gilmore, 1984,

private communication) was observed simultaneously from CFHT in Hawaii and ESO in Chile (Fig. 5b). Also shown for comparison in Fig. 5b is the CTIO observation. The short preimmersion part of the CFHT lightcurve is rather noisy because the observation was made in twilight, low above the horizon (Fig. 5c). A little after midocculta- tion at CFHT, the acquisition was switched from chopping mode to nonchopping mode. This decreased the instru- mental time constant from 0.1 to ~0.025 sec, in the direct acquisition mode. A conspicuous event is visible around the 63,000-km radius at egress (Fig. 5b). The properties of the corresponding ring-like material are investigated in Section 5. This event was simultaneously observed at the Infrared Telescope Facility (IRTF, based about 400 m from CFHT); an analysis of the IRTF data is published elsewhere (Nicholson *et al.* 1990).

This observation led to the detection of a central flash in Chile. This flash is caused by the focusing of rays by Neptune's atmospheric layers around the 0.3-mbar pressure level. This rare phenomenon occurs only if the observer passes within <1000 km of Neptune's shadow center (the impact parameter was about 1100 km for CTIO and ESO on August 20, 1985). The analysis of this flash yields important constraints on Neptune's atmospheric oblateness and methane mixing ratio (Lellouch *et al.* 1986, Hubbard *et al.* 1987b) and on the scintillation in Neptune's stratosphere (Hubbard *et al.* 1987a). Other central flashes were observed on September 12, 1988 at Pic du Midi and on July 7/8, 1989 at ESO (see below). The comparison of these three flashes led to the discovery of the differential rotation of the upper atmosphere of Neptune, and will be published elsewhere (Sicardy *et al.*, in preparation).

3.1.4. April 23, 1986. This is the faintest star that we have observed [N39 on the list of Mink and Klemola (1985), $K = 12.4$; see Table I]. The signal-to-noise ratio is correspondingly one of the lowest (Fig. 5g). Note, how- ever, that the slow speed of the star relative to Neptune (8.2 km/sec) and the use of a large telescope (3.6-m CFH telescope) partly compensate for the faintness.

3.1.5. June 22, 1987. In spite of the relative faintness of the star [n1006 in the list of Nicholson *et al.* (1988), K 10.1), the use of a large telescope (3.6-m ESO telescope), and the excellent meteorological conditions led to a quite satisfactory lightcurve (Fig. 5d). The occultation by the atmosphere of the planet shows very strong spikes (Si- cardy 1988), indicating that the stellar apparent radius projected at the level of Neptune was significantly smaller ($R_* \leq 2$ km, see Section 5) than the typical value of 4–10 km found in the other occultations.

Two secondary events were detected during this obser- vation: one around $3^h44^m5^s$ UTC (near the 53,000-km equatorial radius), and one around $6^h53^m7^s$ UTC, near Triton's orbit (Fig. 1g). The first event, although deep enough, is very short and thus removed very little energy
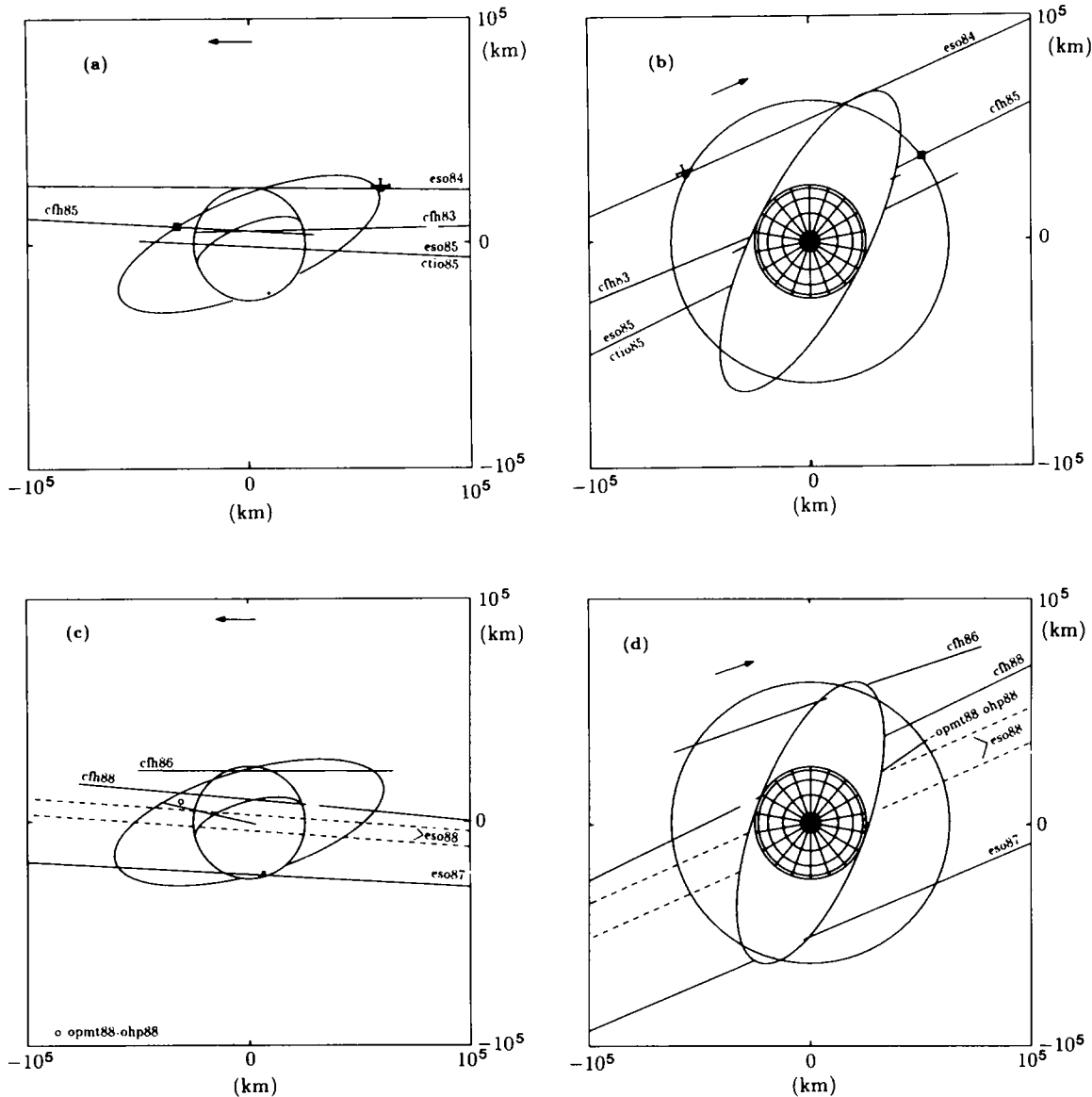
FIG. 1. (a) Star paths, projected in the plane of the sky, for the occultations observed between 1983 and 1985. North is up and East is left. The various orientations of Neptune have been fixed to an average value, using the pole determined by Voyager 2 (Smith *et al.* 1989, and see the text). The tilted ellipse represents an equatorial ring at 63,000 km for the planet's center. The arrow indicates the time evolution. The meaning of the labels are as follows: cfh83: 15 June 1983, CFHT; eso84: 22 July 1984, ESO; eso85–ctio85: 20 August 1985, ESO and CTIO (central flash observed); cfh85: 20 August 1985, CFHT. The dot on the upper right is the location of the event recorded on July 22, 1984 at ESO, with the associated error bar on its position. The square on the left is the location of the August 20, 1985 event of CFHT. For clarity, the small error bar on the position of this event (~200 km) has not been drawn. (b) Same star paths as in (a), but projected in Neptune's equatorial plane. The positive, horizontal x axis, taken as the origin of longitude, is the ascending node of Neptune's equatorial plane on the 1950.0 Earth mean equator. The circle is again the 63,000-km radius. The tilted ellipse is the shadow of Neptune on its own equatorial plane, as observed from the Earth. Any material orbiting inside that ellipse cannot be observed. The arrow indicates the time evolution. (c) Same as in (a), but for the occultations observed between 1986 and 1988. cfh86: 23 April 1986, CFHT; eso87: 22 June 1987 ESO; eso88: 2 August 1988, ESO. The dashed lines are the two possible stellar tracks, neither being preferred because of the prediction uncertainties. cfh88: 25 August 1988, CFHT, the interruption just prior to ingress is due to acquisition problems; ohp88–opmt88: 12 September 1988, OHP and OPMT (central flash observed). (d) Same tracks as in (c), but projected in Neptune's equatorial plane. (e) Same as in (a), but for the 7/8 July 1989 occultation opmt89: 7/8 July 1989, Pic du Midi, the acquisition starts just at 63,000 km because of cloud problems before that time; eso89: 7/8 July 1989, ESO (central flash observed). (f) Same tracks as in (e), but projected in Neptune's equatorial plane. (g) Star paths for some of the occultations, relative to Triton's orbit. cfh83: 15 June 1983, CFHT; eso84: 22 July 1984, ESO; cfh85: 20 August 1985, CFHT; eso87: 22 June 1987, ESO; eso88: 2 August 1988, ESO; cfh88: 25 August 1988, CFHT. The dot is the location of the event recorded near Triton's orbit (see the text), and the cross is the position of Triton when the event was detected.
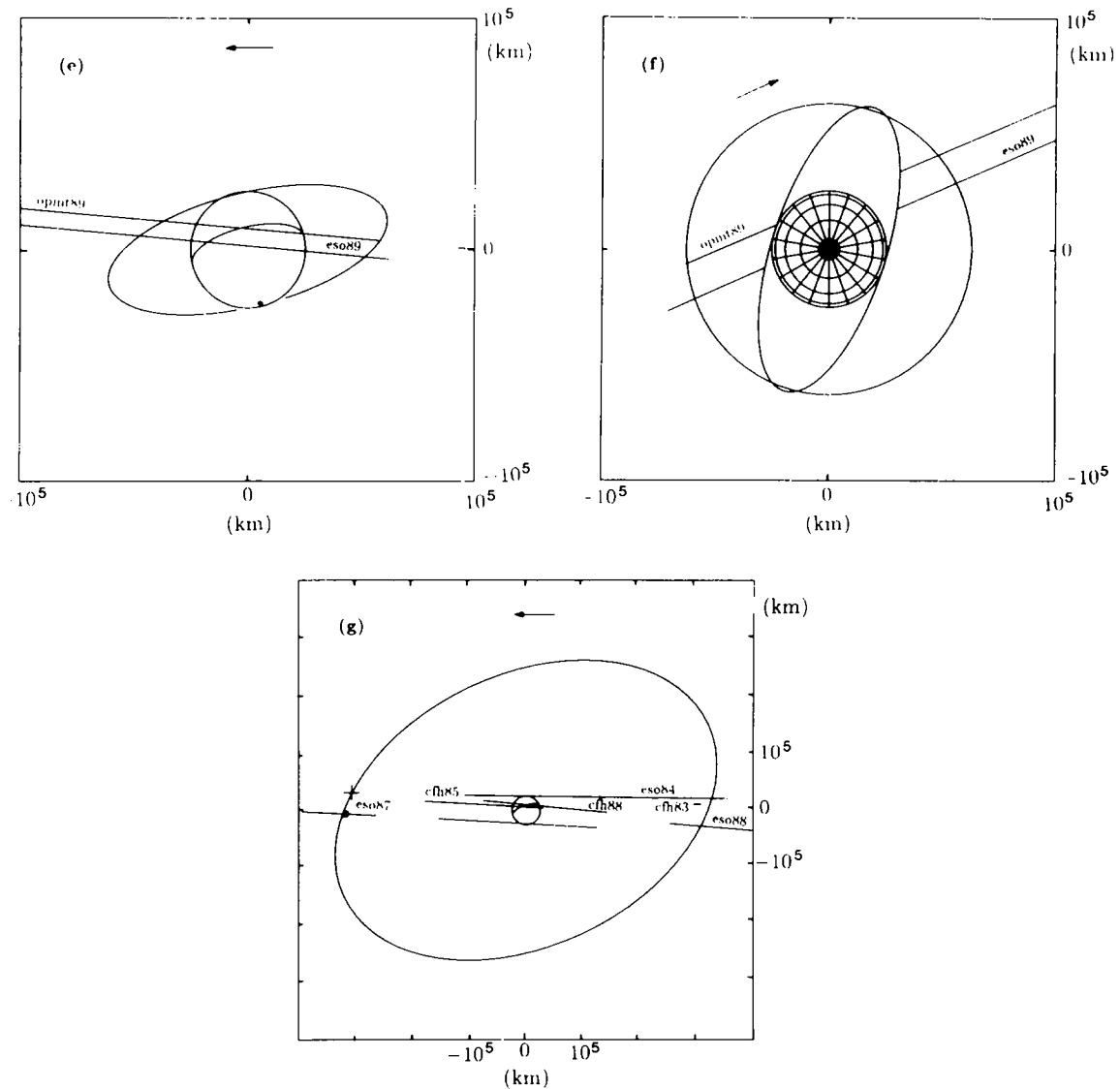
FIG. 1—*Continued.*

from the signal so that it is not visible in Fig. 5d. Its sharpness actually favors an instrumental origin, as we shall see in Section 5 (and see Fig. 4a). The second event may be compatible with material orbiting near Triton's orbit (Fig. 4b).

3.1.6. August 2, 1988. Comparison of this observation [N49 in Mink and Klemola (1985)] with the June 22, 1987 event shows the importance of telescope aperture in the quality of a lightcurve. Both observations were made under approximately the same conditions, considering that the faintness of the star is in one case compensated by the slower motion relative to Neptune (Table 1). The smaller telescope apertures used on August 2, 1988 (1 and 2.2 m

instead of 3.6 m) yield one of the poorest signal-to-noise ratios among all the curves presented here, even on the 2.2-m telescope (Fig. 5e). However, a deep event caused by an opaque body and lasting several seconds could have been detected and confirmed by the 1-m telescope.

Finally, the stellar track was close to central (dashed lines in Fig. 1c), and neither of the two possible solutions is preferred because there are no other observations to decide whether the star passed North or South of Neptune's center. Nevertheless, the midoccultation occurred around 5^h37^m UTC and the miss distance to Neptune's shadow center is about 3560 km for both solutions. There is actually a hint for a faint increase of signal on the 2.2-

m telescope around that time. A more careful analysis could tell if this increase is compatible with the presence of a central flash.

3.1.7. August 25, 1988. In spite of the faintness of the source (n1038 in the Nicholson *et al.* (1988) list, $K = 10.3$), the small velocity of the star relative to Neptune, 11.7 km/sec, yielded a good-quality lightcurve (Fig. 5d). Note that the star scanned well within the Neptune Roche limit, down to a distance of about 33,200 km, i.e., about 1.3 Neptunian radii (Fig. 1d). Note also that about 8 min of data were lost just prior to ingress because of a failure in the acquisition software.

3.1.8. September 12, 1988. The occulted star is candidate N51 in Mink and Klemola's (1985) list, alias n1040 in the Nicholson *et al.* (1988) list. This occultation, the only one visible from Europe in our set with the July 7/8, 1989 occultation, was exceptional because of the brightness of the star ($I = 11.4$, $K = 6.8$) and because of the slowness of Neptune in the plane of the sky ($v_\perp = 3.2$ km/sec). Actually, the occultation occurred only 1 week before the quadrature of the planet (on September 19, 1988). These favorable conditions were, however, counteracted by the modest culmination of Neptune above the horizon (the observation started at $\sim 25°$ and ended at $\sim 9°$). The corresponding lightcurves (Pic du Midi and Haute Provence) are thus of relatively poor quality (see Fig. 5g). The ingress behind the planet occurred during daytime, so that it was not possible to detect it from France. Fortunately, the observation of a central flash in the twilight, just at the beginning of the observation at OPMT, provides good astrometry of the occultation. Finally, a problem in the acquisition software prevented the recording of data during the occultation of the star by the planet at Haute Provence Observatory.

3.1.9. July 7/8, 1989. This is the last occultation observation that we have made prior to the Voyager 2 encounter with Neptune. The very bright infrared source (N55 in Mink and Klemola's list of 1985) has magnitudes $K = 5.5$ and $I \sim 7$, and was observed both at ESO and Pic du Midi. The stellar track in Chile was amost central (Fig. 1e), so that a flash was observed near midocculltation. The conditions of observations in Chile were good; those at Pic du Midi were partially spoiled because of numerous absorptions by clouds. The use of a two-channel photometer, however, allowed us to retrieve most of the signal, by dividing the 0.89-μm channel output (mostly sensitive to the star) by the 0.75-μm channel output (mostly sensitive to Neptune).

3.2. Astrometry Reconstruction

Due to the absolute uncertainty on Neptune's ephemerid and on the star position, it is not possible to know in advance the path of the star relative to the planet with an accuracy better than 0.3–0.5 arcsec, i.e., 6000–10,000 km at the distance of Neptune. Three methods have been used to reconstruct a posteriori the astrometry of each occultation.

When an occultation by Neptune occurs, the half-light times, i.e., the times at ingress and egress when the stellar flux reaches half of its unocculted value, define two points in the plane of the sky. This chord, combined with the known figure of Neptune's shape, gives only two possible trajectories for the star. The ambiguity is in general solved because the predictions are accurate enough to tell whether the star passed North or South of the planet center, except for nearly central occultations (see the August 2, 1988 occultation, Fig. 1c). Information on the orientation of Neptune's disk in the plane of the sky is given in Table I. We have adopted for the Neptunian equatorial radius $a_N = 25,269$ km [pressure level 1 μbar, see Hubbard *et al.* (1987b)], and for the planet's oblateness $\varepsilon = 0.0208$ (Lellouch *et al.* 1986). The error made in the determination of the half-light points essentially comes from the presence of numerous spikes observed during the ingress and egress of the star, thus preventing a rigorous definition of half-light level. Consequently, isothermal synthetic lightcurves are fitted to the data, which defines the half-light times. Note that any deviation from an isothermal profile may introduce systematic errors in the parameters of the best fit. The error made on the determination of the planetary half-light limb is of the order of the scale height H of the probed atmosphere, i.e., about 50 km in the case of Neptune. The half-light times are given in Table III.

TABLE III
Occultation Half-Light Times and Dispersion of the Equivalent Widths

Date	Site	Telescope	Ingress		Egress	
			$t_{1/2}^{(a)}$(UTC)	$\sigma^{(b)}$(m)	$t_{1/2}^{(a)}$(UTC)	$\sigma^{(b)}$(m)
6/15/1983	CFH	3.6-m	$14^h24^m52^s.0$	70	$14^h56^m18^s.5$	-
7/22/1984	ESO	1-m	-	40	-	40
7/22/1984	ESO	0.5-m	-	100	-	100
8/20/1985	CFH	3.6-m	$5^h28^m17^s.0$	85	$6^h41^m18^s.0$	60
8/20/1985	ESO	1-m	$5^h17^m26^s.3$	85	$6^h34^m56^s.1$	290
8/20/1985	CTIO	1.5-m	$5^h17^m31^s.4$	70	$6^h35^m00^s.3$	310
4/23/1986	CFH	3.6-m	$13^h03^m04^s.5$	1550	$13^h34^m50^s.8$	1260
6/22/1987	ESO	3.6-m	$3^h06^m58^s.7$	185	$3^h19^m23^s.5$	185
8/2/1988	ESO	3.6-m	$5^h15^m52^s.8$	1900	$5^h58^m08^s.8$	1900
8/25/1988	CFH	3.6-m	$8^h52^m18^s.7$	260	$9^h57^m51^s.8$	260
9/12/1988	OPMT	2-m	-	-	-	480
9/12/1988	OHP	1.93-m	-	-	-	780
7/7/1989	ESO	2.2-m	$23^h47^m30^s.2$	425	$24^h22^m18^s.7$	170
7/7/1989	ESO	1.-m	$23^h47^m30^s.2$	425	$24^h22^m18^s.7$	425
7/7/1989	OPMT	2.m	$23^h44^m30^s.6$	425	$24^h16^m42^s.7$	425

[a] $t_{1/2}$ is the half-light time of the suboccultation point in Neptune's atmosphere.

[b] σ is the dispersion of E, whose distribution is close to a Gaussian function: $e^{-E^2/2\sigma^2}$. See the text.

A second method has been used if the observer passes within about 1000 km of Neptune's shadow center. In such circumstances, a "central flash" is observed. Such a phenomenon was observed on August 20, 1985 from ESO and CTIO, on September 12, 1988 from OPMT, and on July 7/8, 1989 from ESO. The shape of the flash not only constrains the apparent oblateness of the planet, but also the path of the star relative to Neptune. Again, the error made in such an astrometric reconstruction is roughly one scale-height H.

On July 22, 1984, there was no occultation by Neptune. Thus, only a third method can be used, namely, taking astrometric plates containing both the planet and the star. Three astrometric plates taken and measured by A. Klemola (1984, private communication) at Lick Observatory on June 8, 1984, have yielded a typical accuracy of 0.1–0.2 arcsec, i.e., about 3000–4000 km at the distance of Neptune. Note, however, on Fig. 1a that the nominal track grazed the northern limb of the planet, so that the error in the star position is *not* symmetrical with respect to that nominal track. Closest approach to the northern limb occurred at $6^h 30^m$ + 150 sec UT, with an impact parameter of 25,570 ± 3000 km. Considering Neptune's radius and oblateness at 1 μbar, as well as the geometry of the appulse, an occultation by the planet should have been observed if the impact parameter had been smaller than 24,870 km. Consequently, the error in the star position is, in the vertical direction, $^{+3000}_{-700}$ km. This constraint tightens the error bar on the position of the detected arc, as discussed in Section 5.

The final result of the astrometric reconstruction is the position of the star relative to Neptune, in the plane of the sky, as a function of time. The sky plane coordinates are noted as ξ and η: they define the star position relative to Neptune's center, projected along the local West–East and South–North axes, respectively. The quantities ξ and η are measured positively eastward and northward, respectively. For all the trajectories, we have included in the calculated star position the relativistic corrections due to the bending of starlight by Neptune. The effect of ray deflection reaches about 50 km (in the plane of the sky) near the planet's limb, and decreases as the inverse square of the apparent distance to Neptune's center.

Figures 1a, c, e, and g show the reconstructed astrometries corresponding to our successful observations. We have indicated in these figures the 63,000-km equatorial radius near which we have detected ring-like material and where the Voyager 2 imaging experiment has revealed an arc–ring system (Smith *et al.* 1989). Figures 1b, d, and f show, on the other hand, the stellar tracks projected in the equatorial plane of Neptune. The positive, horizontal x axis defines the origin of longitudes used in this paper. This origin has been chosen to be the ascending node of the equatorial plane on the 1950.0 Earth Mean Equator.

It serves to determine the true longitudes of the detected arcs (see, for instance, Table V). The circles on these figures show again the 63,000-km radius, and the tilted ellipse is the "shadow" of Neptune on its equatorial plane as seen from the Earth. Any ring inside the ellipse is either hidden behind the planet or transiting against the disk. Finally, Fig. 1g shows the full extent of some of our scans out to Triton's orbit. These scans were made whenever possible to search for material outside Neptune's Roche limit, as well as material sharing Triton's orbit.

The nine occultations analyzed here yield 16 independent lightcurves, i.e., lightcurves obtained at different telescopes (see Table I). However, the telescopes at ESO are separated by a distance smaller than the Fresnel diffraction scale and smaller than the stellar diameter, so that they scan identical regions around Neptune. Furthermore, a typical stellar track crosses the Neptune neighborhood twice, once prior to ingress and once after egress. There are three exceptions: the June 15, 1983 occultation yields only a preimmersion lightcurve and the two September 12, 1988 observations each provides only a postemersion lightcurve. Finally the 1-m telescope curve of the August 2, 1988 observation is not used because it is too noisy. Everything considered, we thus obtain 24 independent and separate scans in Neptune's equatorial plane.

4. REDUCTION OF DATA

Our results have been obtained under very different conditions from one observation to another: the impact parameter, the star brightness, and the relative velocities are substantially different among the observations. To readily compare all the lightcurves in spite of these differences, we plot the data on a common radial scale. More precisely, once the astrometry of each occultation is reconstructed, the lightcurve is not plotted versus time, but versus the apparent distance of the star from Neptune's center, projected in the equatorial plane of the planet. Then, the flux is transformed into an "equivalent width" E, roughly defined as the width of an opaque ring which would block as much light as the observed events (see below for details). Finally, when an event is detected, a diffracting bar model is fitted to the profile, to derive such parameters as the physical width of the corresponding ring, its transmission, and its precise location in time.

4.1. Projection in a Reference Plane

To derive a radial scale from the timing t of the lightcurves, the position $\xi(t)$, $\eta(t)$ of the star in the plane of the sky must be projected onto the local Laplacian (reference) plane, where the ring material is assumed to lie. Because of the combined effects of inelastic collisions and the oblateness of the planet, the particles settle into

the reference plane (Brahic 1977, Brahic *et al.* 1982). This reference plane is almost identical to the equatorial plane of the planet for the cases of interest. This is confirmed by the recent Voyager 2 data (Smith *et al.* 1989), which do not show any polar material as predicted by some models (Dobrovolskis 1980, Borderies 1989, Dobrovolskis *et al.* 1989).

Previous interpretations of secondary events around Neptune have been inaccurate due to the error of ~2° in the Earth-based determinations of Neptune's pole (Harris 1984, Jacobson 1987). This resulted in errors of several hundred kilometers when projecting the positions of the secondary events from the sky plane to Neptune's equatorial plane. We use here a "new" pole, as determined by the Voyager 2 Imaging Science experiment (Smith *et al.* 1989). This plane is close to the average orbital plane of the six new satellites discovered during the Voyager encounter. The adopted pole, $\alpha_p = 298°.9$, $\delta_p = 42°.8$ (1950.0), is more precisely defined as the pole which gives the same radius for the arc events detected both from the ground on June 7, 1985 (Covault *et al.* 1986) and August 20, 1985 (see below), and from the spacecraft in August 1989 (Nicholson *et al.* 1990). This new pole is furthermore assumed to be "frozen"; i.e., we neglect the precession of Neptune's pole induced by Triton's orbital precession rate. A conservative estimation of the error attached to Neptune's pole is thus $\Delta\alpha_p \sim \Delta\delta_p \le 0°.1$. Once more accurate values for Triton's mass and orbital elements are known from Voyager 2 data, then together with values of Neptune gravitational moments, the figures given in this paper can be improved.

4.2. Ring Equivalent Width

Once the stellar flux is plotted as a function of the distance r to the planet center in the equatorial plane, then the observed stellar flux $\Phi_*(r)$ is transformed into an "equivalent width" $E(r)$. The calculation of $E(r)$ requires the following steps:

1. An interval of data spanning 1000 km around the radius r is considered. In the middle of this interval, a 50-km window $w(r)$ centered on r is opened, and a linear function $F(\rho)$ is fitted to the data over the 1000-km interval, excluding the 50-km window (ρ is the radius in the window).

2. This linear fit is used to normalize the stellar flux over the 50-km window

$$\phi(\rho) = \Phi_*(\rho)/F(\rho), \tag{1}$$

so that the integrated apparent equivalent width E' of possible ring segments present in the window is

$$E'(r) = \int_{w(r)} [1 - \phi(\rho)]d\rho. \tag{2}$$

3. To obtain a quantity independent of the projection effect, we define

$$E(r) = E'(r) \sin(B) \tag{3}$$

where B is the Neptunocentric elevation of the Earth (see Table 1). The 1000-km interval is then shifted by 50 km, and the procedure is resumed. The result is a plot of $E(r)$ in adjacent 50-km windows.

We note the following:

- The equivalent width E is independent of the stellar diameter or diffraction effects, because these smoothing effects conserve total flux. Furthermore, diffraction of light by small particles yields an overestimation by a factor of 2 of the actual optical depth. This must be taken into account before deriving the ring optical depth (Cuzzi 1985). These corrections are discussed in more detail in Sections 5 and 6.

- For a given observation, the signal-to-noise ratio is highest near the point of closest approach (in the equatorial plane), where many data points are collected in the same 50-km window. Similarly, the best observations are those with the highest value of Φ_*/v_r, where v_r is the radial velocity of the star in the equatorial plane.

- The window method does not assume anything about the *shape* of the events. In particular, artificial events like electric discharges or rapid decenterings are indistinguishable from real events with this method.

- It is important to realize that the choice of a 50-km window is the result of a compromise. It is actually intended to detect *narrow* rings of Neptune, with a width between ~10–20 km (the minimum width allowed by diffraction and the typical stellar apparent diameters) and ≈50 km. Diffuse, wider rings *are canceled out in the present treatment*. This is the desired goal when slow sky variations must be corrected for, but it may overlook the presence of diffuse material around the planet. Such diffuse material is searched for only on the best available lightcurves, i.e., data with photometric quality.

4.3. Diffracting Bar Model

The secondary events are compared to a simple ring model, first to check whether these events are compatible with real ones, and second (if they are real) to determine their geometrical and optical properties. In all the text, the corresponding quantities (width, transmission, optical depth, equivalent width, and equivalent depth) are primed when they are "apparent," i.e., when the arc is observed

projected in the plane of the sky, and nonprimed when they are "normal," i.e., when the arc is observed perpendicularly to its own orbital plane. Finally, a subscript d is used when diffraction effects are taken into account (see below).

Our approach for modeling the data is the "square-well" model described by Elliot *et al.* (1984):

- The ring-like material is modeled as a uniformly gray strip, bounded by sharp edges.
- The model includes the diffraction of the wavefront by the strip, and then convolves the profile by the filter bandpass, by the stellar apparent disk, assumed to be uniform (i.e., there is no limb darkening), and finally by the instrumental response.

The algorithm used for generating the diffraction paterns of the strip allows us to calculate the Fresnel functions, and thus the diffraction profiles, with an arbitrary accuracy (Roques *et al.* 1987). The synthetic profile is then fitted to the observed profile, using a standard least-squares simplex method. Following are the free parameters of the model:

- the mid-time, t_0 of the event;
- the radial width, W_r, of the strip, projected in the plane of the ring;
- The *apparent* (i.e., in the plane of the sky) fractional transmission f' of the profile [the quantity f' is defined as the fraction of energy going through the ring, and is related to the apparent optical depth τ' by $\tau' = -\ln(f')$];
- the flux just outside the ring profile [this flux may not coincide with the full unocculted stellar flux since there can exist faint diffuse material around the ring; this is the case, for instance, for the arc profile detected on August 20, 1985 at CFHT (see Section 5 and Fig. 3c)].

The stellar apparent radius R, is not taken as a free parameter, but rather is set to some fixed value at the beginning of each fit. Then, the effect of R, is investigated "by hand" for minimizing the residuals. This approach is dictated by the complex topology of the residuals when the stellar radius is varied. In particular, it may appear that the residuals have several local minima, with no possibility of deciding which minimum is the best one. This is the case for the August 20, 1985 arc event, for which two solutions are possible (Section 5 and Figs. 3a, b).

It should be kept in mind that the square-well model is somewhat arbitrary, and would probably not be expected on theoretical grounds. Rather, it is a convenient model, with the smallest possible number of free parameters, which allows a homogeneous comparison of all the observed profiles. Such a description allows also the determination of model-independent quantities like the "equiv-

alent width" E and the "equivalent depth" A. The two distances E and A are defined as (Elliot *et al.* 1984)

$$E = W_r(1 - f')\sin(B)$$
$$A = W_r\tau'\sin(B). \tag{4}$$

The quantity E is proportional to the total amount of light removed from the stellar beam, i.e., the surface occupied by the particles if the ring is observed normally *and* if the ring is semitransparent and monolayer. The quantity A, on the other hand, is proportional to the total amount of material present in a vertical section of the ring *if* the latter is polylayer. Note, however, that these two quantities coincide for low-optical-depth rings and diverge from each other for dense rings. With the normal optical depth found for the arcs in this paper (in the range 0.03–0.07, see Table IV), E and A differ by less than about 10%. Physically, E may be interpreted as the radial width of an opaque monolayer ring which would block as much light as the observed ring, when both are observed perpendicularly to the ring plane. On the other hand, A may be interpreted as the radial width of a multilayer equatorial ring, with normal optical depth unity, which would contain as much material as the observed ring.

Finally, one must note that a uniform gray screen with fractional transmission f' is *not* equivalent to a particulate ring with free fractional area f', when it is observed from far. This is because each particle creates its own diffraction pattern, thus scattering the incident wave on a spatial scale much larger than the width W_r. This leads to an overestimation of the actual optical depth τ' by a factor 2 (Cuzzi 1985). Thus, the actual normal optical depth τ_d, the equivalent width E_d, and the equivalent depth A_d at the distance of Neptune are, once diffraction effects are taken into account,

$$\tau_d = \tau'\sin(B)/2$$
$$E_d = W_r(1 - f'_d)\sin(B) \tag{5}$$
$$A_d = A/2,$$

where $f'_d = e^{-\tau_d^2} - \sqrt{f'}$.

5. ARC DETECTIONS

We pointed out in the introduction that several secondary events have been observed in addition to the occultations by the planet. Most of them can easily be identified as artifacts due to electrostatic discharges, poor seeing, decentering, clouds, or other artifacts. We present in this section three events for which such explanations do not hold. Two of these events have been observed from three

TABLE IV
Optical and Geometrical Properties of the Secondary Events

Date and site	v_r (km/s)	B	R_* (km)	t_o (UTC)	$W_r^{(a)}$ (km)	f'	$E_d^{(b)}$ (km)	$A_d^{(b)}$ (km)	$\tau_d^{(b)}$
July 22, 1984 ESO	-18.94	$-19°.261$	8.5	$5^h40^m08^s.7$	15.1	0.64	1.	1.1	0.074
August 20, 1985 CFHT	16.84 "	$-19°.84$ "	5.75 3.5	$6^h53^m49^s.1$ "	15.3 25.2	0.71 0.82	0.8 0.8	0.9 0.8	0.058 0.034
					W'	f'	E'	A'	τ'
June 22, 1987 ESO[c]	24.09	-	(0.05)	$(3^h44^m05^s.5)$	(0.9)	(0.16)	(0.2)	(0.3)	(0.92)
"	24.07	-	0.3	$6^h53^m06^s.9$	10.1	0.84	0.3	0.3	0.087

[a] W_r is the radial width of the event, projected in Neptune's equatorial plane.

[b] The values of E_d, A_d, and τ_d have been corrected for the viewing geometry and the factor of 2 due to particle diffraction. See the text. Note, however, the exception for the June 22, 1987 observation.

[c] All the primed quantities associated with this observation are projected in the plane of the sky. See the text. Quantities in parentheses are associated with the probably instrumental event of June 22, 1987.

and two telescopes, on July 22, 1984 at ESO and August 20, 1985 at CFHT, respectively. They correspond to material orbiting inside Neptune's Roche limit, and they led to the preparation and the achievement of the Voyager 2 ring observations. The third event, observed near Triton's orbit (June 22, 1987 at ESO), remains ambiguous because of the lack of a simultaneous detection. As an example, we describe also a fourth event (observed on June 22, 1987 at ESO, around the 53,000-km radius) that can be discarded based on our diffracting bar model.

5.1. July 22 1984, ESO

The July 22, 1984 observation led to the first unambiguous detection of incomplete ring-like material around Neptune (Hubbard *et al.* 1986). Such a conclusion is based on the following arguments:

• The event was observed simultaneously by three independent telescopes: the 0.5-m and 1-m telescopes at ESO and the 0.9-m telescope at CTIO, 100 km away from ESO. This rules out spurious events like clouds, power failure, acquisition problems, etc.

• The event is well fitted by a square-well diffracting bar model at the distance of Neptune (Fig. 2a). Furthermore, the relative location of ESO and CTIO in the plane of the sky shows that the detected material is locally aligned with a Neptunian equatorial ring. This argues for material associated with the planet, rather than material

close to Neptune in the sky, but at a very different distance.

• The width of the occulting body is about 15 km (Table IV), while its length is at least 100 km (i.e., the separation between ESO and CTIO). Furthermore, the profiles of the two events are similar, considering the noise level. This rules out an occultation due to a small Neptunian satellite, unless a very special geometry occurred. Finally, no event was detected on the same night when the radius of the assumed equatorial material was crossed again (Fig. 2b). In any case, other observations do not show any significant events at that radius, thus ruling out the presence of dense, permanent continuous rings around Neptune.

These points lead to strong evidence for the presence of ring-like material around Neptune, with a highly inhomogeneous azimuthal distribution.

A least-squares fit to the 0.5-m telescope event is shown in Fig. 2a. We do not study here the 1-m telescope profile, because the chopping rate was significantly lower on the 1-m telescope (7 Hz) than on the 0.5-m telescope (100 Hz), and so the profile needs deconvolution and will be presented elsewhere. The variation of the residuals as a function of the apparent stellar radius R_* indicates that effective stellar radii between ~7.3–7.8 and ~8–8.5 km are equally possible. The variations of W_r, f', and t_0 when R_* is varied from 7.3 to 8.5 km are typically 0.1 km, 0.01, and 0.01 sec, respectively. This corresponds to a typical error in the normal optical depth τ_d of ~0.003 (with diffrac-
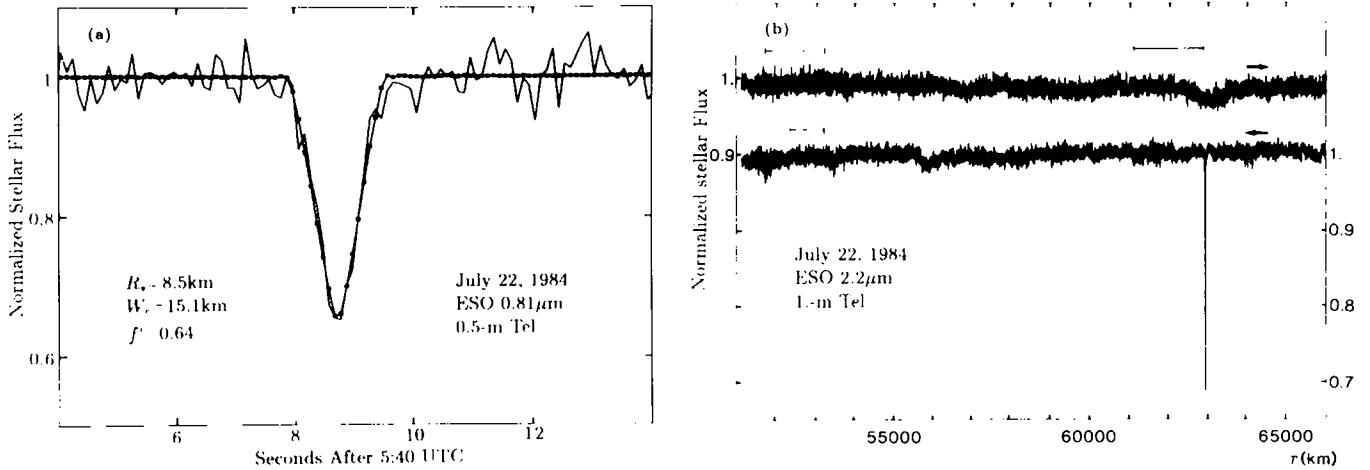
FIG. 2. (a) Best fit of a semitransparent diffracting bar model to the 22 July 1984 arc profile (0.5-m ESO telescope). The quantities R, W_r, and f' are respectively the stellar apparent radius, the ring radial width (projected in the plane of the ring), and the ring apparent fractional transmission (see the text). (b) Stellar flux at the 1-m telescope where the stellar track again crosses the arc orbit (upper curve). The lower curve shows the arc. The data are averaged on 1-km intervals. The arrows indicate the time evolution and the horizontal bars indicate where the crossings of the 53,200- and 63,000-km radii occur, within the astrometric uncertainties.

tion taken into account). The values of W_r, f', and t_0, as well as the derived optical depth, and the equivalent width and depth E_d and A_d are summarized in Table IV.

The timing of the events provides its location relative to Neptune. However, since no occultation by the planet occurred (Fig. 1a), the astrometry relies only on astrometric plates, with typical errors of ±3000 km. This error translates directly onto the distance of the detected arc from the planet's center (Table V). The situation is more favorable for determining the true longitude L of the arc in Neptune's equatorial plane. As discussed in Section 3.2, the stellar track can be shifted by at most 700 km to the south; otherwise an occultation by the planet would have taken place. This constant explains why the error bar on L in Table V is *not* symmetrical with respect to zero.

TABLE V
Locations of the Arcs

Date and site	$\xi^{(a)}$ (km)	$\eta^{(a)}$ (km)	$r^{(b)}$ (km)	$L^{(b)}$
July 22, 1984 ESO	-60290 ± 3000	24900 $+\frac{3000}{700}$	65300±3000	$151°.6 \pm\frac{3}{7}$
August 20, 1985 CFHT	32275 ± 50	8090 ± 50	63160±200	36°.8±0.2

[a] ξ and η are the coordinates of the arc in the plane of the sky, relative to Neptune's center.

[b] r and L are the radius and the longitude of the arc in Neptune's equatorial plane, respectively. See the text for details.

5.2. August 20, 1985, CFHT

This occultation, simultaneously observed from Chile and Hawaii, led to the second unambiguous detection of arc material from Mauna Kea in Hawaii (Fig. 5b). Note also on Fig. 5b that *no* event was recorded on the same night on the other side of the planet, from ESO and CTIO.

Figure 3 displays some details of the Hawaii event, together with least-squares fits to the data. A map of the residual in a width-transmission (W_r, f') grid reveals that, for a given apparent stellar radius R, there are actually two local minima, whose relative depths depend on R. Consequently, there are two branches of solutions for the best fit. The best fits corresponding to each branch are displayed in Figs. 3a and b, respectively. With solution 1, we have $R = 5.75$ km, $W_r = 15.3$ km, and $\tau_d = 0.058$ with typical errors on W_r and τ_d of 0.2 km and 0.001, respectively. These error bars are estimated from the quality of various fits near the best least-squares fit. Solution 2 yields $R = 3.50$ km, $W_r = 25.2 \pm 3$ km, and $\tau_d = 0.034 + 0.001$ (Table IV). One can see that these two fits give essentially indistinguishable profiles, and have essentially identical equivalent widths, from the conservation of energy. A similar conclusion is reached by Nicholson *et al.* (1990) with the simultaneous IRTF observations.

Note that with solution 1, the detected body has the same width as the July 22, 1984 arc ($W_r = 15.1$ km). The scintillation of the stellar flux in Neptune's atmosphere may add some independent constraints on the stellar diameter, thus discriminating between solutions 1 and 2. Narayan and Hubbard (1988) have developed a model of turbulent scintillation which allows one to retrieve the stellar dimension from the spikes observed during the
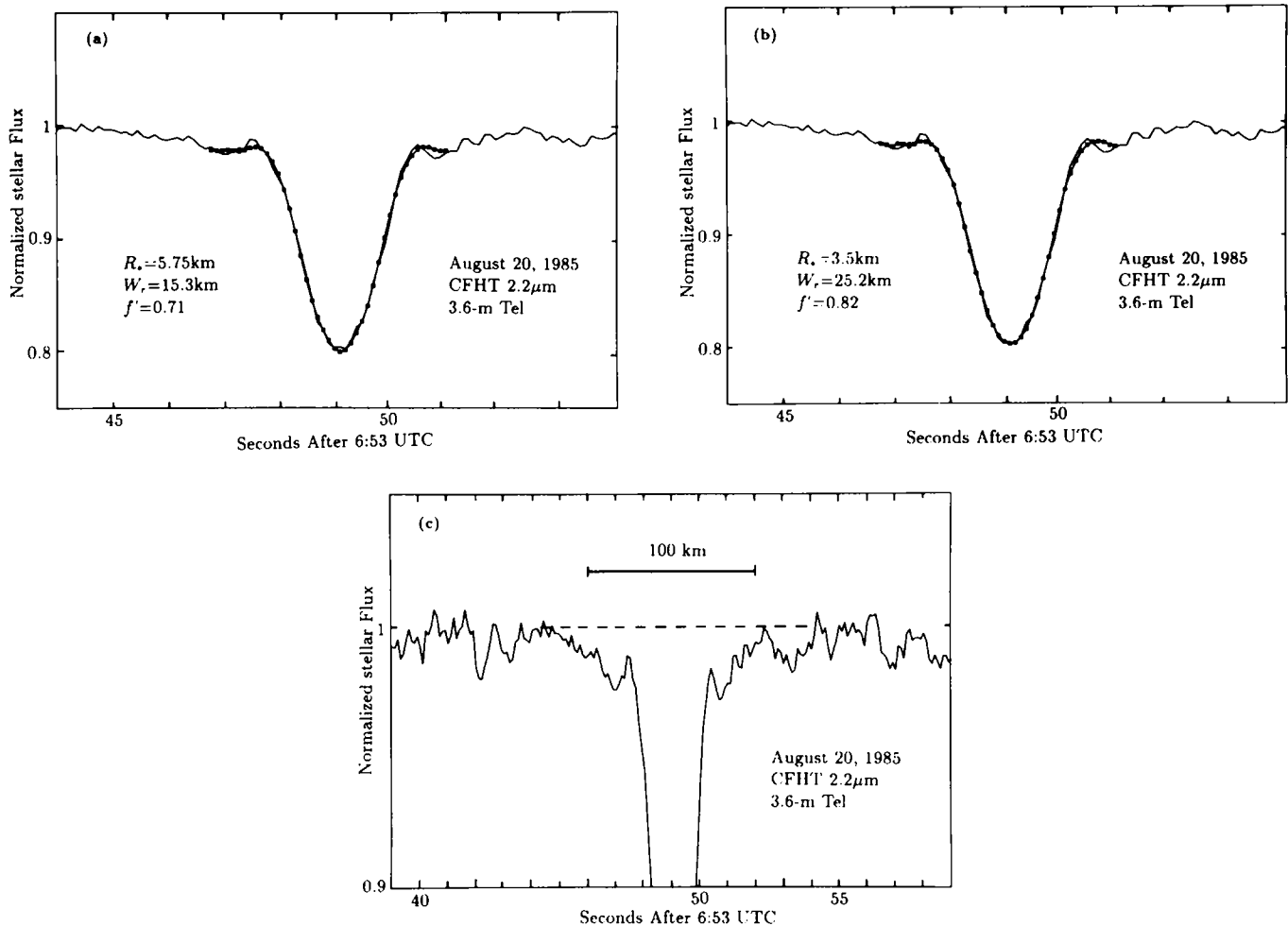
FIG. 3. (a, b) Fits to the August 20, 1985 arc profile (CFHT). Two equally satisfying solutions are possible, depending on the assumed apparent stellar radius R_*. Note that the flux does not reach unity just outside the arc profile, which betrays the presence of diffuse material. (c) Possible diffuse material associated with the 20 August 1985 arc profile (CFHT). An approximately 1.5% signal drop is visible around the main feature, extending approximately ≤100 km from edge to edge, in the equatorial plane of Neptune. This profile may be compared to the simultaneous arc profile detected at the nearby IRTF station (Nicholson *et al.* 1990).

occultation by the planet's stratosphere. Assuming a Gaussian intensity distribution, these authors derive a typical effective radius (1σ dispersion) of $\sigma_* = 4.7$ km for the star. This dispersion roughly corresponds to a radius $R_* \sim 6$ km for an uniformly bright stellar disk. Thus this result seems to favor solution 1 over solution 2; i.e., it favors the solution which yields the same width as the July 22, 1984 event.

The August 20, 1985 object has a size which is not very large compared to the Fresnel scale $\sqrt{\lambda D/2} \sim 3$ km, where λ is the wavelength and D is the distance between the observer and the diffracting object. The width W_r is also comparable to the apparent stellar diameter ~ 12 km, so that it is actually difficult to distinguish between a diffraction pattern caused by a semitransparent bar and that caused by a small opaque satellite (Roques *et al.* 1987).

However, the present profile exhibits some shoulders (Fig. 3c), showing the presence of faint material around the main object. This argues for the object being composed of semitransparent ring material rather than being a single compact body.

The typical apparent optical depth of this faint material is $\tau_0 \sim 0.015$, corresponding to a normal optical depth $\tau_d \sim 0.0025$. The typical total width of the arc plus its shoulders is ≤100 km (Fig. 3c). Comparison with the arc profile detected simultaneously at IRTF confirms the existence of the inner shoulder, with similar optical depth and width, but does not confirm the presence of the outer shoulder (Nicholson *et al.* 1990). A careful comparison of the noise levels and instrumental responses on the respective curves could explain the origin of this discrepancy.

The geometrical and optical properties of the dense part

of the arc are summarized in Table IV. Table V provides the radius r and longitude L of the detected body. The quoted errors are due partly to the uncertainty on the astrometry (about one scale height, ~50 km, as discussed in Section 3.2) and partly to the uncertainty of Neptune's pole position ($\Delta\alpha_p$ ~ $\Delta\delta_p$ ~ 0°.1, see Section 4.1). The geometry of the occultation is such that the dependence of r on α_p and δ_p is almost identical in this case,

$$\partial r/\partial\alpha_p \sim \partial r/\partial\delta_p \sim 1650 \text{ km/deg}. \tag{6}$$

from which we derive an error Δr ~ +200 km. A similar analysis, applied to the longitude L, yields ΔL ~ ± 0°.2.

5.3. The June 22, 1987 Events, ESO

The two events presented here offer a good example of the weakness of claims based on observations with only one telescope. A partial answer to this problem is the use of diffracting bar models to distinguish between real and spurious events. Despite this, some events remain ambiguous, as seen below.

5.3.1. An instrument event? During this observation, made at ESO under excellent transparency and seeing conditions, a secondary event was recorded inside the Roche limit of the planet, at 52,800 ± 200 km from Neptune's center (Fig. 4a). Attempts were made to fit the diffraction model to this very narrow event. Figure 4a presents one of the best fits, obtained by shifting all the parameters so as to decrease the duration of the synthetic event. In particular, the star was considered as essentially a point source (R. = 0.05 km), and the object was assumed to be perpendicular to the stellar track. The only smooth-

ing effects are thus diffraction and the instrumental response. The resulting synthetic profile is still too shallow, and its inbound slope is not steep enough compared to the observed drop of signal. The physical parameters associated with this event are found in Table IV. Note that they refer to apparent quantities, since no attempt was made to project the dimensions of the putative object in a particular reference plane.

A possible explanation for this event is an electrostatic discharge on the detector, a phenomenon which can cause very sharp variations of signal, in both positive and negative directions.

5.3.2. The Triton event. An appulse between the star and Triton (closest approach ~ 2 arcsec), occurred about 3 hr 30 min after the closest approach to Neptune (Fig. 1g). No occultation by Triton occurred, but a secondary event was observed as the star passed near Triton's orbit, in the plane of the sky (Fig. 4b). This event is referred to as the "Triton event." The crossing of Triton's orbit occurred near the culmination of Neptune at ESO, at a zenithal distance of only 23°. This circumstance, combined with the good stability of the signal, the absence of guiding problems, and the uniqueness of the event during the 90 min of observation around the appulse, argues for a real event.

A fit to the data is shown in Fig. 4b; see also Table IV, where again the quantities are apparent. As for the previous event, we have assumed that the occulting bar was perpendicular to the star track, and note that the best fit requires a rather small apparent stellar diameter (R. ~ 0.3 km). However, it appears that any value of R. ~ 2 km yields an equally satisfactory fit, considering the noise level. This small apparent radius seems to be compatible
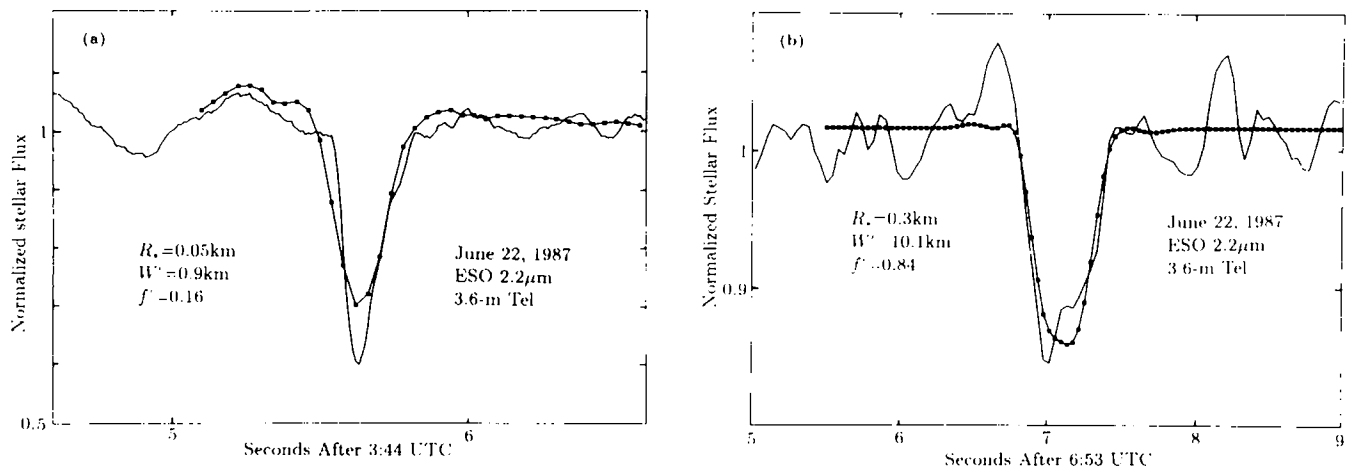
FIG. 4. Two events observed during the 22 June 1987 occultation at ESO. In this figure, W' is the apparent width of the event, projected in the plane of the sky. See the text. (a) This deep and sharp event is probably spurious because it is narrower than allowed by diffraction and instrumental smoothing effects. In this fit, the star is assumed to be essentially a point source, and the diffracting bar is assumed to be normal to the stellar track. (b) The event detected near Triton's orbit. Note the change of vertical scale with respect to the previous figure. The diffracting model can now fit both the slope and the depth of the event.
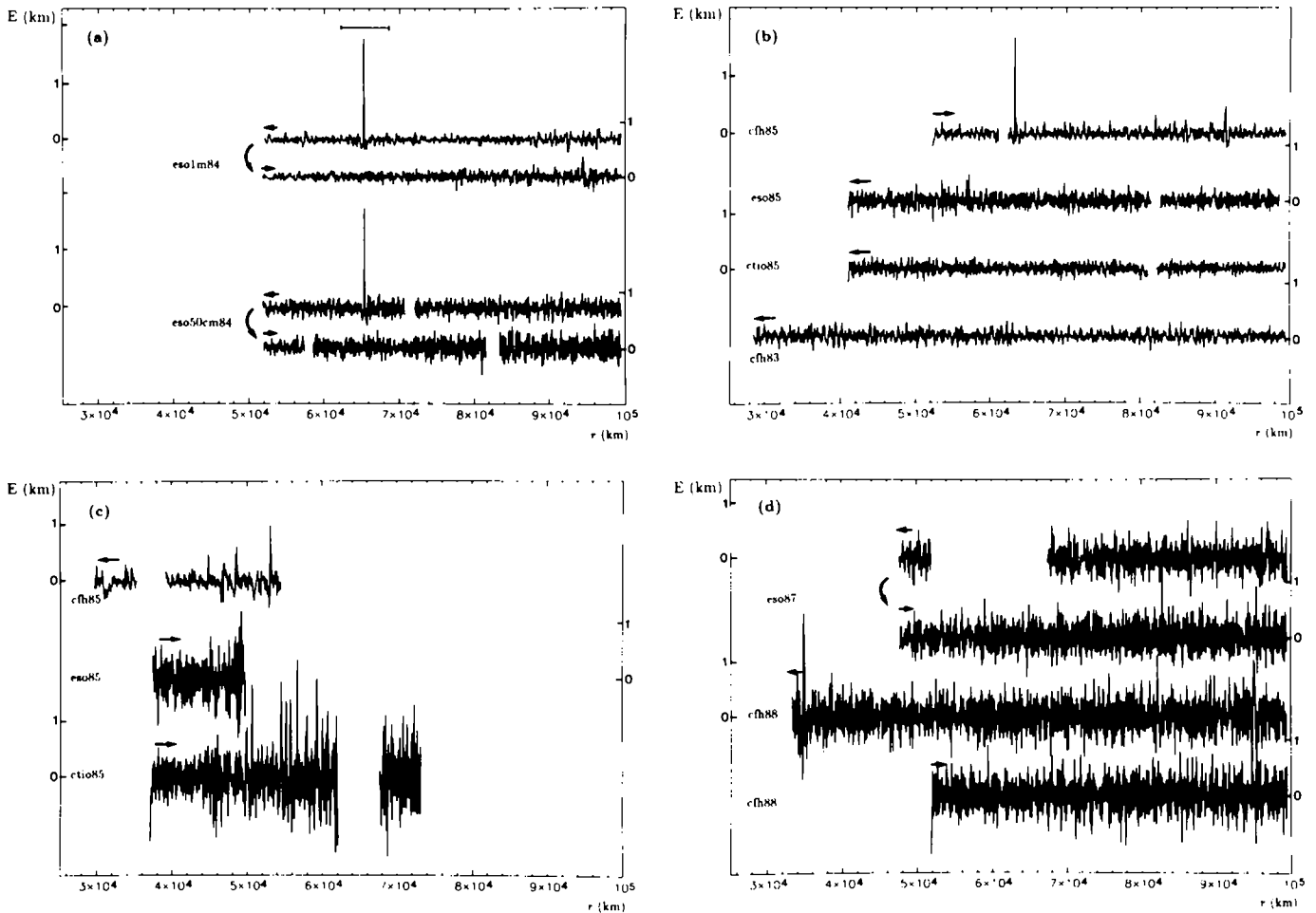
FIG. 5. Stellar flux, transformed in equivalent width E(see the text), as a function of the distance r to Neptune's center, in the equatorial plane of the planet. The curve labels refers to the year and the observatory. The arrows indicate the time evolution. Most of the observations have a preimmersion curve (←) and a postemersion curve (→). A vertical, bent arrow indicates a continuity in the data, when the minimum distance to the planet center is not reached behind the disk of Neptune, but in the plane of the sky. (a) to (d) have the same vertical scale, while the poorer data of (g) have a compressed vertical scale. (a) eso1m84: 22 July 1984, ESO 1-m telescope, before and after the minimal distance to the planet's center. eso50cm84: Same plots, but for the ESO 0.5-m telescope. Note that the star was not occulted by the planet, so that there is continuity between the curves. The error bar indicates the uncertainty on the radial scale near the detected arc, due to the astrometry uncertainty. (b) Same in (a). 20 August 1985 preimmersion data observed from the CFH 3.6-m telescope cfh85 and postemersion data observed from the ESO 1-m telescope (eso85) and the CTIO 1.5-m telescope (ctio85). Note the conspicuous arc detection near 63,000 km in the CFHT data. The event near 92,000 km is due to a recentering. See the text and Fig. 3 for more detail on the arc detection. cfh83: Preimersion data of 15 June 1983 observed from CFHT (there are no postemersion data). (c) Same as in (a). 20 August 1985 data, 3.6-m telescope. cfh85: CFHT preimmersion. The data are noisier than the postemersion ones because they were recorded during twilight and lower above the horizon. eso85 and ctio85: postemersion data observed from the ESO 1-m telescope and the CTIO 1.5-m telescope, respectively. These data are noisier than the preimmersion data because they were recorded lower above the horizon. (d) Same as in (a). eso87: 22 June 1987 ESO, 3.6-m telescope, before and after the minimum distance to the planet center, which happens here before the immersion. cfh88: 25 August 1988 preimmersion and postemersion data observed from the CFH 3.6-m telescope. (e) Same as in (a) eso2m89: 7/8 July 1989 ESO, 2.2-m telescope, preimmersion and postemersion data. eso1m89: 7/8 July 1989 ESO, 1-m telescope, preimmersion data. The postemersion data were lost because of an acquisition problem. (f) Same as in (a). opmt89: 7/8 July 1989 OPMT, 2-m telescope, preimmersion and postemersion data. (g) Same as in (a), but note the change of vertical scale. cfh86: 23 April 1986 CFH, 3.6-m telescope, before and after the closest approach to the planet center, which happens after the emersion. eso88: 2 August 1988 ESO, 2.2-m telescope, preimmersion and postemersion data. We assume here that the star passed south of the planet center; see Fig. 1c. opmt88 and ohp88: 12 September 1988 postemersion data from the OPMT 2-m telescope and the OHP 1.93-m telescope, respectively. There are no preimmersion data because it was then daytime.

with the very high spikes observed during the ingress and egress of the star in Neptune's stratosphere (Sicardy 1988). The narrowest spikes have a duration at half-height of ~0.27 sec, while the velocity of the star perpendicular to the planet's limb is 9.1 km/sec, from which we derive a typical stellar radius of ~1.5 km. An analysis similar to
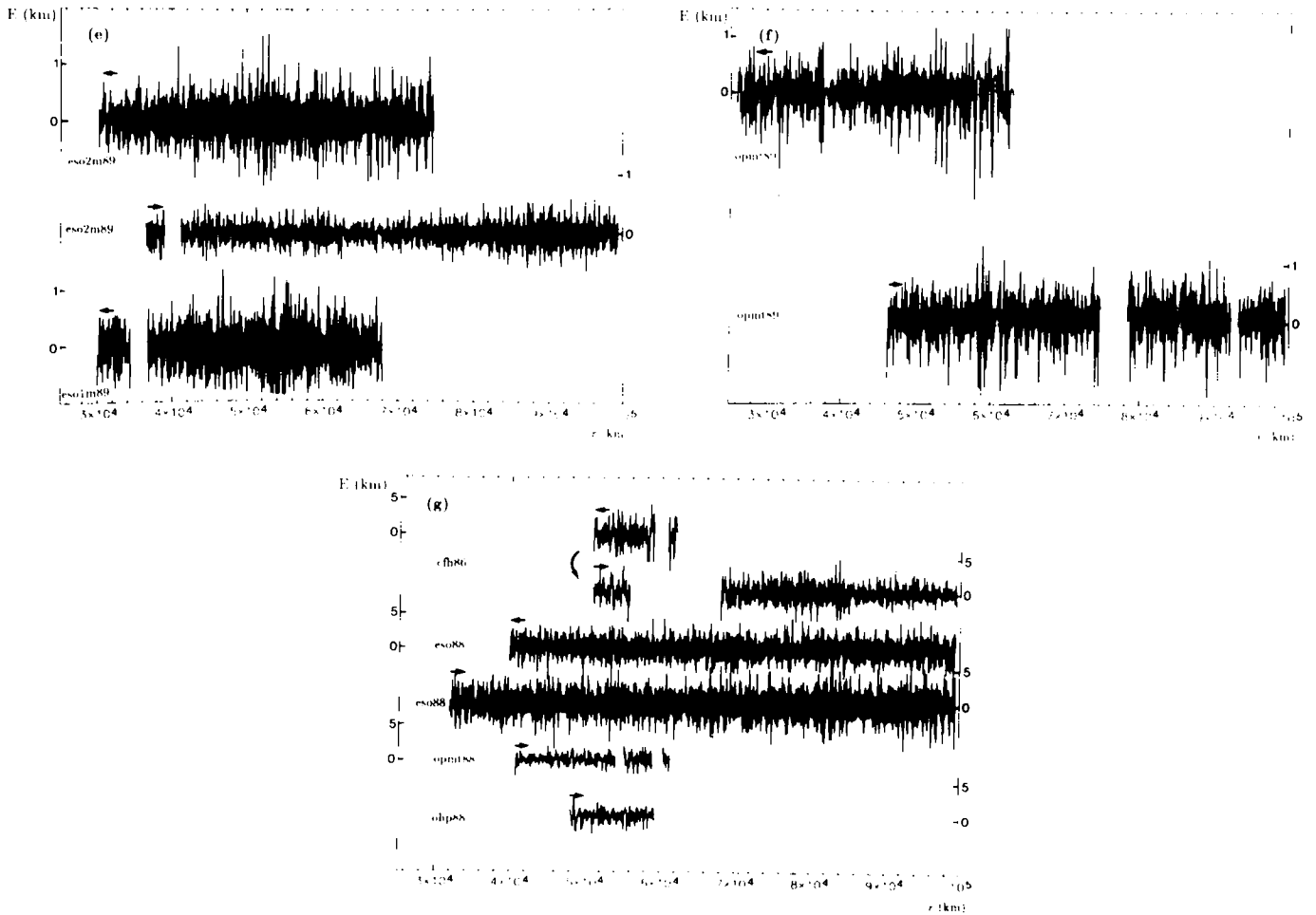
FIG. 5—*Continued*

that of Narayan and Hubbard (1988) could actually better constrain the stellar diameter, and thus provide some ground for confirming or refuting the reality of this event.

Figure 1g shows the position of the Triton event relative to the satellite. If projected in Triton's orbital plane, the putative body would lie 245,800 km from Neptune's center, i.e., about 8500 km inside Triton's orbit (whose semi-major axis is $a_T = 254,290$ km), and would be leading the satellite by about 5°. As far as we know, there was no simultaneous, independent observation of this particular occultation, so that there is no firm confirmation of the Triton event.

6. DETECTION LIMIT FOR ADDITIONAL MATERIAL

In this section, we present the plots of the equivalent width E as a function of the distance r from the planet's center (see Section 4.2), for all our observations. These

"reduced lightcurves," which allow a homogeneous comparison of all the data, do not show any obvious events, except of course for the two arc detections previously described. A systematic study of these data will be done in paper II. As we have pointed out in Section 4.2, the window method used to derive the reduced lightcurves is adapted to detect *narrow* Neptunian rings, up to a width of ≈ 50 km, *not* for studying wider rings. These wider rings, which may be confounded with low-frequency variations of the sky tranparency, should be searched for only on the data with the best photometric quality.

As explained in Section 3.2 the nine occultations analyzed here yield 24 independent and separate scans in Neptune's equatorial plane. These scans are displayed in Fig. 5. The best lightcurves are displayed in Figs. 5a–f, and the lower-quality data are found in the remaining Fig. 5g. The explored region has been limited to a distance of 10^5 km from Neptune's center.

For each reduced lightcurve, we calculate the distribution of the apparent equivalent width $E(r)$, which can then
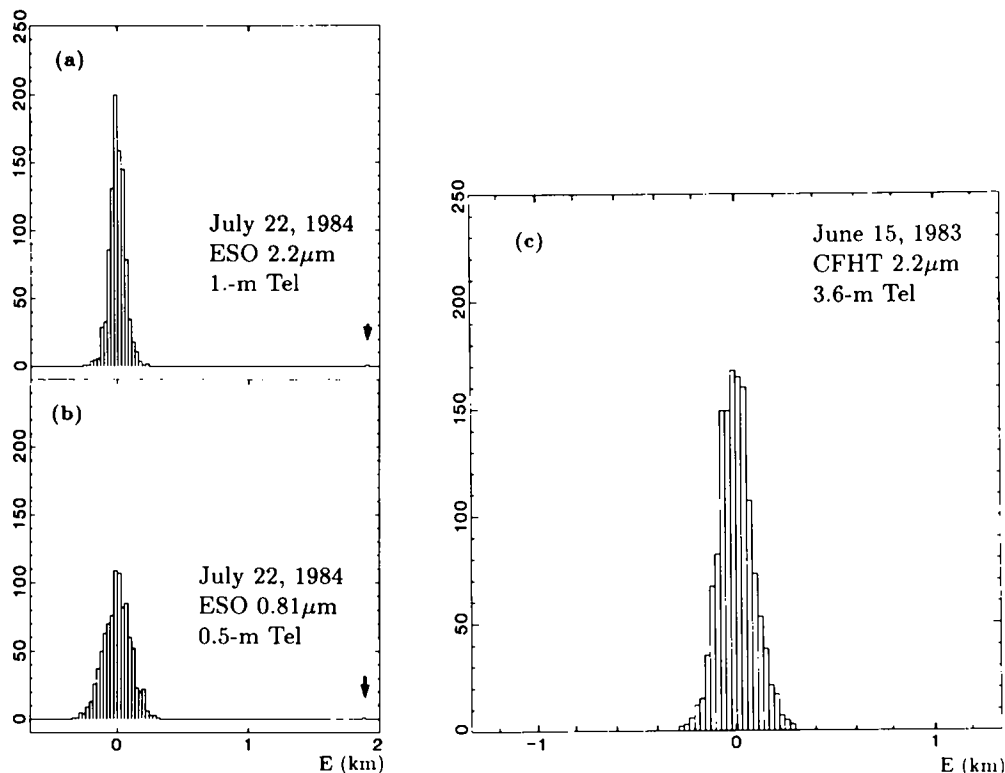
FIG. 6. Histogram of distribution of the equivalent width E. (a) 22 July 1984, 1-m ESO telescope. No positive events with equivalent width larger than 230 m are observed, except for the arc detection at $E = 1.8$ km (arrow). (b) 22 July, 1984, 0.5-m ESO telescope. The wider distribution in the histogram compared to (a) is caused by the larger noise on the original lightcurve. In this histogram, there is no positive event with an equivalent width larger than 330 m, except again for the arc at 1.8 km. (c) Same as in (a) and (b), but for the 15 June 1983 occultation observed at the CFH 3.6-m telescope. This histogram has been calculated by pooling together all the points of curve cfh83 of Fig. 5b, i.e., considering distances spanning the interval ~28,000–100,000 km in the planet's equatorial plane (~1.1–3.95 Neptunian radii). Thus, this histogram represents, in our set, the best coverage of Neptune's equatorial plane as far as continuous rings are searched for.

be plotted as a histogram. The histograms derived from the various reduced lightcurves are found to follow approximately the normal law; i.e., the frequency of occurrence of an event with width E is proportional to $e^{-E^2/2\sigma^2}$. A refined analysis of the noise in the occultation lightcurves will be done elsewhere. The root-mean-square dispersion σ is a constant which depends on the conditions of observation, and is consequently a direct illustration of the quality of the lightcurve: the smaller the σ, the better the detection limit for a Neptunian ring. Table III gives the dispersion σ for each of our reduced lightcurves, while Fig. 6 shows, as our best examples, the histograms corresponding to the July 22, 1984 data (1- and 0.5-m telescopes, ESO) and the June 15, 1983 data (3.6-m telescope, CFH).

Table III shows substantial differences in the quality of the occultation lightcurves. We can define three groups, according to this quality:

Group 1: June 15, 1983, August 20, 1985 (CFHT, ESO and CTIO), and July 22, 1984. These lightcurves have a

σ of less than 100 m and they will be used to set an upper limit for continuous rings around Neptune.

Group 2: August 25, 1988, June 22, 1987, and July 7/8, 1989 have a σ of about 200 m. These lightcurves would have allowed the detection of the arcs observed in 1984 and 1985.

Group 3: August 2, 1988, April 23, 1986, and September 12, 1988. These lightcurves have a dispersion of the order of 1 km. They allow the detection of only very deep events, and the arcs detected in 1984 and 1985 would have appeared only as 2σ events in these data.

Simple preliminary considerations give a good idea of this detection limit. First, we give the detection limit obtained from our best two reduced lightcurves (June 15, 1983 and July 22, 1984), taken separately. Then, the four reduced lightcurves of group 1 are used to search for correlated events. Finally we will use the best raw data of July 22, 1984 to set an upper limit on the optical depth of the continuous rings detected by Voyager 2 near the 63,000- and 53,000-km radii.

6.1. Detection Limit from Individual Lightcurves

The lowest dispersion reduced lightcurve is from the July 22, 1984 occultation (1-m telescope). Figure 5a shows that the arc apparent equivalent width $E = 1.8$ km is well above the largest event caused by noise (about 230 m). The dispersion σ of this lightcurve is 40 m. A lower limit of detectability can thus be set at the 5σ level, i.e., $E_{lim} = 200$ m. One must be careful, however, in interpreting the significance of this figure, since the the 5σ detection limit also depends on the nature of the noise, which may not be Gaussian. The statistical analysis presented in paper II shows in particular that the noise becomes non-Gaussian for large events. Finally, if the searched rings are polylayer and have a low optical depth, the factor 2 correction due to diffraction applies, and yields a 5σ detection level of $E_{lim,d} = 100$ m.

The June 15, 1983 reduced lightcurve does not have such a good dispersion, with $\sigma = 70$ m. However, the scan is more complete since it goes down to $r \sim 28,000$ km in the equatorial plane ($1.1R_N$). The corresponding normal upper limit (again at the 5σ detection level) for continuous rings is then $E_{lim} \sim 350$ m, or $E_{lim,d} \sim 175$ m when diffraction is taken into account.

6.2. Limit on Real Events from Correlated Detection

6.2.1 General Comparison of the Best Lightcurves.

A real event has been defined as a confirmed signal drop, appearing at least twice at the same distance from the center of the planet, either simultaneously on two telescopes, or on both sides of the planet during one observation, or during two different occultations. So, we have used the reduced lightcurves of group 1, except for the 1984 ones, to search for simultaneous events (the 1984 lightcurves are not used here because of their larger astrometric error). The deepest events on these lightcurves have an equivalent width of roughly 300 m, i.e., six times less than the arcs. We have noted on these lightcurves the events appearing on at least two lightcurves at the same radius, with a possible shift of 400 km due to astrometric errors. We have taken into account roughly 40 events on each lightcurve, corresponding to events with E greater than roughly 100 m. This comparison allows us to state the following:

- The deepest event appearing on at least two lightcurves at the same radius has an equivalent width of about 200 m ($r = 57,690$ km, $E = 180$ m on the ESO 1985 lightcurve and $r = 57,650$ km, $E = 200$ m on the CTIO 1985 lightcurve; see Fig. 5b).
- Furthermore, we have noted that near $r = 55,300$–$55,700$ km, there were events appearing on all the four reduced lightcurves. These events have equivalent widths E in the range 160–270 m, or $E_d \sim 80$–135 m with

the factor 2 due to diffraction. As we shall see in the next subsection, however, these simultaneous detections may be regarded as due to noise only.

In conclusion, we cannot claim the detection of correlated events except of course for the 1984 and 1985 arcs. Our upper limit on such possible events is $E_{lim} \sim 200$ m, or $E_{lim,d} \sim 100$ m when diffraction by individual particles is accounted for.

6.2.2. Search for ringlets around 53,200 and 63,000 km.

We use here the data obtained by the Voyager 2 spacecraft to undertake a more local search around the two radii where the Imaging Science Experiment has revealed the presence of continuous rings, i.e., at $r \simeq 63,000$ km and $r \simeq 53,200$ km [Smith et al. (1989); see also Section 7]. On each reduced lightcurve, we define an interval where the ring observed by Voyager 2 would be expected. The width of this interval takes into account the astrometric errors, as discussed in Sections 3.2 and 5.2.

We would like here to estimate the threshold of detectability of continuous ringlets, i.e., of simultaneous events. More precisely, we are going to estimate the probability $P(E)$ that, due to noise only, there is in each of the intervals of data at least one data point which is above the threshold E. For $E \ll 0$, $P(E)$ tends to unity since all the data have values near zero. When E is increased to positive values, $P(E)$ decreases until the probability that the noise produces simultaneous, large events becomes vanishingly small. Thus, $P(E)$ provides the threshold E_{lim} above which a simultaneous detection may be considered as real (i.e., not due to noise).

The value of $P(E)$ around a given radius r is estimated in the following manner. First, we consider the best reduced lightcurves, labeled i. From a given lightcurve i, we extract an interval containing N points around the radius r, where the ring should be. The astrometric errors are typically ± 200 km when an occultation takes place, and approximately ± 3000 km when there is only an appulse (see Sections 3.2 and 5). Since the reduced lightcurves have a sampling step of 50 km, this yields $N = 8$ points in the first case and $N = 120$ points in the second case. Second, let $f_i(E)$ be the density of probability of occurrence of E in the lightcurve i. Then, for one data point, the probability that E is larger than the threshold E_0 is

$$p_i(E_0) = \int_{E_0}^{\infty} f_i(E)dE. \tag{7}$$

Thus, the probability that among the N_i data points bracketing r on lightcurve i there is at least one with $E > E_0$ is

$$P_i(E_0) = 1 - [1 - p_i(E_0)]^{N_i}. \tag{8}$$

since $[1 - p_i(E_0)]^{N_i}$ is the probability that all the values of E in the interval are smaller than E_0.

Finally, the probability of each of the considered intervals showing at least one event with $E > E_0$ is

$$P(E_0) \approx P_1(E_0) \times P_2(E_0) \times \ldots \times P_i(E_0) \times \ldots , \quad (9)$$

where the product is extended over all the considered lightcurves. These calculations assume that all the data points are uncorrelated and that the various lightcurves are uncorrelated as well. This is a reasonable assumption as long as the sampling step of the reduced lightcurves (50 km, i.e., typically 2 sec of time or more on the raw curves) is somewhat larger than (i) the instrumental response and (ii) the typical seeing fluctuation time, which are both a fraction of a second.

The calculation of the respective functions $f_i(E)$ in Eq. (7) is thus the last problem that we have to solve. Unfortunately, the exact noise statistics of each lightcurve are not known, for at least two reasons: (i) the noise is a combination of instrumental noise, seeing effects, and possible decenterings; the physics of each of these effects is not sufficiently controlled to derive theoretical statistics of the noise, (ii) In any case, the noise on a given lightcurve is continuously changing due to varying observational conditions (elevation of the star, variability of the seeing, etc.). Thus the densities of probability f_i have to be approximated by the observed distributions of E, which are nothing other than the histograms of E (see, e.g., Fig. 6). To be significant, however, the sample of data points from which these histograms are derived must be large enough. Nevertheless, it must not be too large; otherwise, remote parts of the lightcurve, where the noise level is significantly different, would bias the statistics near r. We have taken, as a compromise, intervals of 5000 km around the reference radius r, in order to approximate f_i. Thus, we have used 100 data points for each histogram, i.e., about 8 min of recording if the typical stellar relative velocity is 20 km/sec.

The final result, i.e., the estimation of $P(E)$ around the two radii 53,200 and 63,000 km, is shown in Fig. 7. For each of the radii, we have used four reduced lightcurves, namely, the June 15, 1983 data of CFHT, the July 22, 1984 data of ESO, and the August 20, 1985 data obtained at ESO and CTIO. The July 22, 1984 data, which have a large astrometric uncertainty ($\pm$ 3000 km), are a priori less constraining, since the probability that a wide interval contains at least one event larger than E increases rapidly with the number N of points in the interval [see the expression of P_i in Eq. (7)]. However, because of its good photometric quality, the July 22, 1984 lightcurve yields a cutoff of P_i for $E \geq 120$ m and, thus, a cutoff for $P(E)$ as well near that value (Fig. 7).

Figure 7 also shows that the estimated probability $P(E)$ steadily decreases from unity at $E = 0$ to zero at ≈ 120 m. More precisely, above $E \approx 150$ m, $P(E)$ drops to zero for
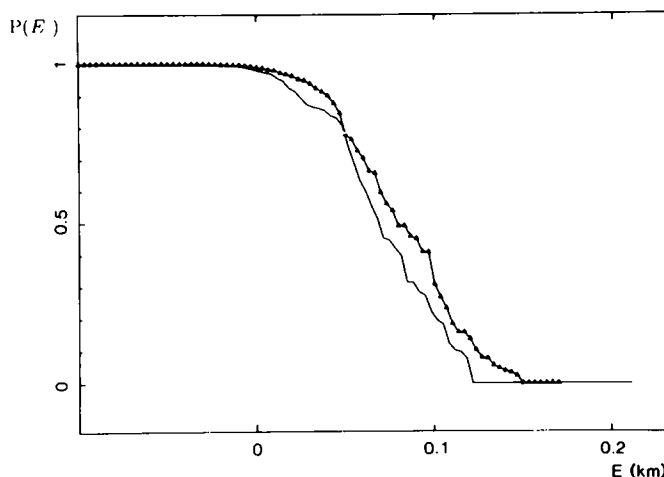
FIG. 7. Plots of the probability $P(E)$ that the noise produces simultaneously an event larger than E on the reduced lightcurves of June 15, 1983 (CFH 3.6-m telescope), July 22, 1984 (ESO 1-m telescope), and August 20, 1985 (ESO 1-m telescope and CTIO 1.5-m telescope). The solid line refers to the probability near the 63,000-km radius and the solid line with triangles refers to the probability near the 53,000-km radius. See the text for details.

events occurring near 53,200 km while it drops to zero at $E \approx 110$ m for events occurring near 63,000 km. The latter limit is slightly better than the former because the noise on the July 22, 1984 reduced lightcurve is smaller near 63,000 km than near 53,200 km (Fig. 5a). Figure 8a is an enlargement of the three reduced lightcurves for which we have good astrometry, near the radius 53,200 km. There is no evidence for a simultaneous event larger than ≈ 150 m in the ring region. The same is true near the 63,000-km radius (Fig. 8b).

In conclusion, we can say conservatively that the largest events (with, however, a physical width smaller than $W \sim 50$ km; see Section 4.2), observed simultaneously near the the 53,200- and the 63,000-km radii, on the four reduced lightcurves studied here, have an equivalent width of $E \sim 150$ m, or $E_d \sim 75$ m if diffraction is taken into account. On the other hand, the frequency of simultaneous occurrence of events rises sharply under this limit, due to noise (Fig. 7). In other words, *all these events can be explained by noise only*. In particular, the correlated events with $E_d \sim 80$–135 m noted near 55,500 km (Section 6.2.1) cannot be regarded as significant.

6.3. Limit of Material on the July 22, 1984 Arc Orbit

Because of its good photometric quality, the July 22, 1984 lightcurve (1-m telescope) has been used to search for diffuse material in the orbit of the 63,000-km arc. If we suppose that a ring is associated with the orbit of the August 20, 1985 arc ($r = 63,160$ km), and if we take into account the astrometric uncertainty on the July 22, 1984 lightcurve, then we deduce that a ring sharing the arc's
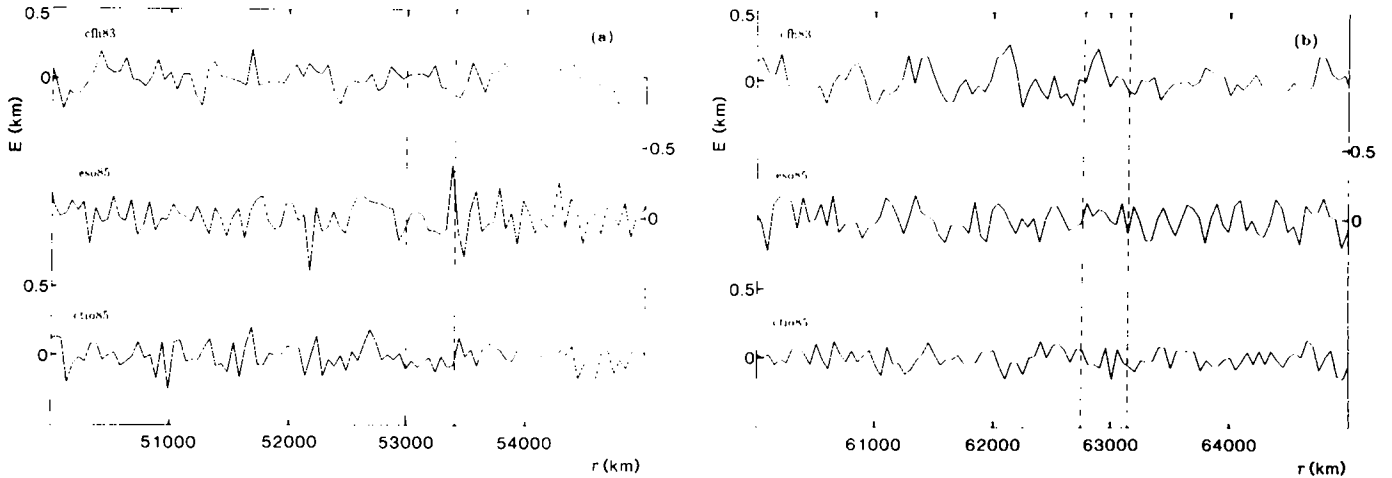
FIG. 8. (a) Enlargement of Fig. 5 around the 53,200-km radius, where Voyager 2 detected a continuous ring sharing the arc orbit. cfh83: June 15, 1983. CFH 3.6-m telescope. eso85: August 20, 1985. ESO 1-m telescope. ctio85: August 20, 1985. CTIO 1.5-m telescope. The dashed lines show the location of the ring taking the astrometrical errors into account. (b) Same as Fig. 8a, but around the 63,000-km radius.

orbit should be observed in the interval shown in Fig. 2b, where the stellar flux has been averaged on 1-km intervals. As a matter of fact, a wide shallow event is visible near 63,000 km (at $\sim 6^h 20^{mn}$ UTC). The depth of this event gives an upper limit of $\tau \sim 8 \times 10^{-3}$ for the normal optical depth of material associated with the 63,000-km arc, where again we have taken into account the viewing geometry. If the factor of 2 caused by particle diffraction is considered, this limit becomes $\tau_d \sim 4 \times 10^{-3}$. A closer search for narrow events near the 63,000-km radius does not show any drop with $\tau_d > \sim 4 \times 10^{-3}$. Note, however, that this limit applies as long as we can resolve spatially the ring. Our limit of resolution is roughly the stellar apparent diameter, i.e., ~ 15 km for the July 22, 1984 observation. The minimum equivalent width that we can detect is thus $\sim 4 \times 10^{-3} \times 15$ km $- 60$ m. This value is comparable to the limit of 75 m derived in the previous section. Finally, a similar search near the 53,000-km radius yields the same upper limit of $\tau_d - 4 \times 10^{-3}$ (see Fig. 2b).

The limit $\tau_d \sim 4 \times 10^{-3}$ is significantly smaller than the estimation of the optical depth ($\tau \sim 0.01$–0.02) of the continuous ring observed by the Voyager near the 63,000-km radius (Smith *et al.* 1989). This apparent discrepancy is discussed in the next section, in view of the assumptions made to derive this figure, and considering also that the ring was not resolved on the Voyager images.

7. DISCUSSION

7.1. Results of the Present Work

The present set of observations yields evidence for incomplete, or at least highly inhomogeneous, ring-like ma-

terial around Neptune and it gives an upper limit for the density of continuous rings of the planet.

We have two firmly confirmed detections of material around Neptune, one from the July 22, 1984 observation and the other one from the August 20, 1985 observation. Our analysis shows that these events were most probably caused by highly inhomogeneous ring-like material, or arcs, orbiting the planet. Considering the error associated with the position of the arc detectd in 1984, these two detections are compatible with a unique orbit at $r = 63,160 \pm 200$ km from the planet's center. Also, the geometrical and optical properties of these two arcs are rather similar. In particular, the equivalent width and depth E and A of both events are in the range 0.8–1.1 km (Table V). If solution 1, described in Section 5, is chosen for the best fit to the August 20, 1985 arc profile, then even the physical radial widths of the two events are identical, at $W_r \sim 15.2$ km. Finally, from the July 22, 1984 observations, we can claim that the arc is at least 100 km long (distance from ESO to Cerro Tololo projected in Neptune's equatorial plane).

We have searched in the remaining data for *narrow* continuous rings, i.e., rings with a width in the range 10–50 km. Our observations show no evidence for such ringlets between 1.1 and 3.5 Neptunian radii, down to a 5σ limit for E of about 350 m, for the equivalent width (or 175 m if diffraction is taken into account). A more local search for coincident events shows no ringlets with E larger than about 150 m (or 75 m if diffraction is taken into account) near the 53,200- and 63,000-km radii, where the Voyager 2 spacecraft observed two continuous rings.

Finally, there are no diffuse rings with normal optical depth greater than about 4×10^{-3} near these two radii,

and it will be shown in paper II that the frequency of arc detection from the ground implies a azimuthal filling factor of about 10%.

7.2. Other Ground-Based Observations

Several secondary detections during stellar occultations by Neptune have been reported by different groups. The first confirmed event occurred during the 24 May 1981 appulse to Neptune, and was observed by two telescopes. It was first interpreted as the discovery of the third satellite of Neptune (Reitsema *et al.* 1982). It can be interpreted as being due to a satellite of at least 100 km in diameter or by an opaque ring of about 80 km in width, orbiting at about three Neptunian radii ~75,000 km (Hubbard 1986), i.e., further away than the July 1984 and the August 1985 arcs. Now, the locations of these events actually seem to be consistent, in both radius and longitude, with the satellite 1989N2 recently discovered on the Voyager 2 images (Smith *et al.* 1989). Another event is reported by Nicholson *et al.* (1990) from the 18 April 1984 occultation observed at Palomar Observatory. It would correspond to material orbiting 55,140 ± 125 km from Neptune's center, with a width of 9.2 km and a normal optical depth of 0.14, i.e., an equivalent width close to those of the arcs presented here. However, this event was observed with only one telescope, and therefore is not presently confirmed.

Finally, the occultation of a binary star on June 7, 1985 also led to the detection of a sharp secondary event, again with a single telescope (Covault *et al.* 1986). Its radius, r = 62,853 ± 27 km, is compatible with the arc distance observed by Voyager 2 (Nicholson *et al.* 1990), and compatible also with our arc radius of r = 63,160 ± 200 km.

7.3. The Voyager 2 Observations

Thanks to the observations reported above, the Voyager 2 spacecraft was reprogrammed and successful observations by the imaging system revealed a complete ring system and three arcs around Neptune (Smith *et al.* 1989).

More precisely, it appears that Neptune possesses two narrow, unresolved rings near the 53,200- and 63,000-km radii, a wide and faint plateau extending halfway between these two rings, and a resolved (Δr ~ 1700 km) diffuse ring about 42,000 km for the planet's center. Embedded in the 63,000-km ring are three conspicuous arc structures, sharing the same orbit and keeping the same relative positions, at least on a scale of a few weeks. The total azimuthal extension of the arc system is about 35°, each arc spanning approximately 4°, 4°, and 10°. We propose the names Liberty, Equality, and Fraternity, respectively, for these three features.

The two confirmed arc detections presented in this paper are thus compatible in radius with the arcs detected

by Voyager near the 63,000-km radius (Fig. 1a), while the azimuthal extension observed by the spacecraft agrees, in order of magnitude, with the frequency of detection from ground-based occultations. Since the highest-resolution images of Voyager 2 do not resolve the arc width, it is not possible to compare the geometrical and optical properties observed from the Earth and from the spacecraft. Meanwhile, the PhotoPolarimeter Science experiment, which detected one of the arcs by means of a stellar occultation, also gives a profile compatible with those presented here, with a radial width of W_r ~ 9-11 km, a normal optical depth of τ ~ 0.05, and an equivalent depth of A ~ 0.8 km (Lane *et al.* 1989). A similar conclusion is reached by the UltaViolet Spectrometer observations, with an equivalent depth A = 0.66 ± 0.12 km (Broadfoot *et al.* 1989).

The optical depth of the continuous ring associated with the arcs is estimated to be in the range 0.01-0.02, from the analysis of the Voyager 2 images (Smith *et al.* 1989), while we give in this paper an upper limit of τ_d = 4 × 10^{-3}, with diffraction effects taken into account. Note, however, that the figure derived from the Voyager 2 data comes from the total light *scattered* by the 63,000-km ring, assuming it has the *same* width (W_r = 15 km) as the arc, and assuming also a Bond albedo ω_0 ~ 0.01-0.02 for the large particles of the ring. What is actually measured from the spacecraft images is the total amount of light scattered by the arc, a quantity proportional to $\omega_0 W_r \tau = \omega_0 E$. Thus, the equivalent width of the 63,000-km ring scales like E ~ $30/\omega_0$ m. On the other hand, our upper limit of τ_d = 4 × 10^{-3} is based on the *transmitted* light only. As noted in Section 6.3, this limit applies as long as we can resolve the ring, so that we could not detect rings with equivalent width smaller than ~60 m. This can be reconciled with the Voyager results if ω_0 is larger than about 0.5. However, before any conclusion about the particle albedo is driven, a homogeneous analysis of both sets of data is now necessary to see if this discrepancy is real or due, on the contrary, to the assumptions made in each approach.

More generally, a careful comparison between all the ground-based and space observations will obviously be most fruitful. First, a complete analysis of the Voyager 2 imaging and navigation data will provide a better definition of Neptune's equatorial plane and precession rate. The initial step toward careful comparison of the longitudes of the ground-based observations with the Voyager results has been discussed by Nicholson *et al.* (1990), confirming the Smith *et al.* (1989) results. Second, both the positive and negative ground-based observations, spanning a time interval of several years, can tell where the arcs were, or were not, during that time, which will address the important problem of the arc stability. Preliminary results indicate that the observed mean motion of the arcs, as determined by the Voyager 2 observations, is indeed in

agreement with the arc longitudes determined by ground-based observations (Smith *et al.* 1989). This suggests that the arc structures are stable over at least 5 years. Finally, the knowledge of the arc mean motion allows one to predict whether a given ground-based stellar occultation by an arc will occur. In particular, coordinated efforts could be made for such observations, to check the arc stability and also to study its azimuthal variations from site to site.

ACKNOWLEDGMENTS

REFERENCES

BHATTACHARYYA, J. C., AND K. KUPPUSWAMY 1977. A new satellite of Uranus. *Nature* **267**, 331–332.

BORDERIES, N. 1989. Properties of possible polar rings around Neptune. *Icarus* **77**, 135–147.

BRAHIC, A. 1977. Systems of colliding bodies in a gravitational field. I. Numerical simulation of the standard model. *Astron. Astrophys.* **54**, 895–907.

BRAHIC, A. 1982. Neptune est-elle entourée d'anneaux? *Recherche* **13**, 413–415.

BRAHIC, A. 1985. Qu'y a t-il autour de Neptune? *Recherche* **16**, 834–836.

BRAHIC, A., B. SICARDY, AND S. CLAIREMIDI 1982. Perturbations of collisional particles discs. *Bull. Amer. Astron. Soc.* **14**, 750.

BRAHIC, A., AND W. B. HUBBARD 1989. The baffling ring arcs of Neptune. *Sky Telescope* **77**, 606–609.

BRAHIC, A., B. SICARDY, W. B. HUBBARD, F. ROQUES, A. BARUCCI, C. FERRARI, M. FULCHIGNONI, I. GRENIER, J. LECACHEUX, J. P. MAILLARD, C. PERRIER, AND B. A. SMITH 1990. Neptune's rings and arcs. Submitted for publication.

BRAHIC, A., B. SICARDY, F. ROQUES, R. MCLAREN, AND W. B. HUBBARD 1986. Neptune's arcs: Where and how many? *Bull. Amer. Astron. Soc.* **18**, 778.

BROADFOOT, A. L., S. K. ATREYA, J. L. BERTAUX, J. E. BLAMONT, A. J. DESSLER, T. M. DONAHUE, W. T. FORRESTER, D. T. HALL, F. HERBERT, J. B. HOLBERG, D. M., HUNTEN, V. A. KRASNOPOLSKY,

S. LINICK, J. I. LUNINE, J. C. MCCONNEL, W. H. MOSS, B. R. SANDEL, N. M. SCHNEIDER, D. E. SHEMANSKY, G. R. SMITH, D. F. STROBEL, AND R. V. YELLE 1989. Ultraviolet spectrometer observations of Neptune and Triton. *Science* **246**, 1459–1466.

COVAULT, C. E., AND L. M. FRENCH 1986. JHK photometry of Uranus and Neptune occultation candidate stars: 1986–1990. *Icarus* **66**, 630–631.

COVAULT, C. E., I. S. GLASS, R. G. FRENCH, AND J. L. ELLIOT 1986. The 7 and 25 June 1985 Neptune occultations: Constraints on the putative Neptune "arc." *Icarus* **67**, 126–133.

CUZZI, J. N. 1985. Rings of Uranus: Not so thick, not so black. *Icarus* **63**, 312–316.

DOBROVOLSKIS, A. R. 1980. Where are the rings of Neptune? *Icarus* **43**, 222–226.

DOBROVOLSKIS, A. R., N. BORDERIES, AND T. Y. STEIMAN-CAMERON 1989. Stability of polar rings around Neptune. *Icarus* **81**, 132–144.

ELLIOT, J. L., E. W. DUNHAM, AND D. MINK 1977a. The rings of Uranus. *Nature* **267**, 328–330.

ELLIOT, J. L., R. G. FRENCH, E. DUNHAM, P. J. GIERASH, J. VEVERKA, C. CHURCH, AND C. SAGAN 1977b. Occultation of ε Geminorum by Mars. II. The structure and extinction of the Martian upper atmosphere. *Astrophys. J.* **217**, 661–679.

ELLIOT, J. L., R. G. FRENCH, K. J. MEECH, AND J. H. ELIAS 1984. Structure of the Uranian rings. I. Square-well model and particle-size constraints. *Astron. J.* **89**, 1587–1603.

ELLIOT, J. L., D. J. MINK, J. H. ELIAS, R. L. BARON, E. DUNHAM, J. E. PINGREE, R. G. FRENCH, W. LILLER, P. D. NICHOLSON, T. J. JONES, AND O. G. FRANZ 1981. No evidence of rings around Neptune. *Nature* **294**, 526–529.

FRENCH, R. G., J. L. ELLIOT, AND S. E. LEVINE 1986a. Structure of the Uranian rings. II. Ring orbits and widths. *Icarus* **67**, 134–163.

FRENCH, R. G., J. L. ELLIOT, L. M. FRENCH, J. A. KANGAS, K. MEECH, M. RESSLER, M. W. BUIE, J. A. FROGEL, J. B. HOLBERG, J. F. FUENSALIDA, AND J. MARSHALL 1988. Uranian ring orbits from Earth-based and Voyager occultation observations. *Icarus* **73**, 349–378.

FRENCH, R. G., J. A. KANGAS, AND J. L. ELLIOT 1986b. What perturbs the γ and δ rings of Uranus? *Science* **231**, 480–483.

GUINAN, E. F., C. C. HARRIS, AND F. P. MALONEY 1982. Evidence for a ring system of Neptune. *Bull. Amer. Astron. Soc.* **14**, 658.

HARRIS, A. 1984. Physical properties of Neptune and Triton inferred from the orbit of Triton, *in Uranus and Neptune.* In *Proceedings of a workshop held in Pasadena, CA, Feb. 6–8, 1984.* NASA conference publication 2330. pp. 357–373.

HUBBARD, W. B. 1986. 1981 N1: A Neptune arc? *Science* **231**, 1276–1278.

HUBBARD, W. B., A. BRAHIC, B. SICARDY, L. R. ELICER, F. ROQUES, AND F. VILAS 1986. Occultation detection of a Neptunian ring-like arc. *Nature* **319**, 636–640.

HUBBARD, W. B., E. LELLOUCH, B. SICARDY, A. BRAHIC, F. VILAS, P. BOUCHET, R. A. MCLAREN, AND C. PERRIER 1987a. Structure of scintillation in Neptune's occultation shadow. *Astrophys. J.* **325**, 490–502.

HUBBARD, W. B., P. D. NICHOLSON, E. LELLOUCH, B. SICARDY, A. BRAHIC, F. VILAS, P. BOUCHET, R. A. MCLAREN, R. L. MILLIS, L. H. WASSERMAN, J. H. ELIAS, K. MATTHEWS, J. D. MCGILL, AND C. PERRIER 1987b. Oblateness, radius, and mean stratospheric temperature of Neptune from the 1985 August 20 occultation. *Icarus* **72**, 635–646.

JACOBSON, R. A. 1987. *Satellite Ephemerides for the Voyager Neptune Encounter.* AAS/AIAA Astrodynamics Specialist Conference, Kalispell, MT, August 10–13, 1987, paper AAS 87-464.

JEWITT, D. C., G. E. DANIELSON, AND R. J. TERRILE 1981. Ground based observations of the Jovian ring and inner satellites. *Icarus* **48**, 536–539.

LANE, A. L., C. W. HORD, R. A. WEST, L. W. ESPOSITO, K. E. SIMMONS, R. M. NELSON, B. D. WALLIS, B. J. BURATTI, L. J. HORN, A. L. GRAPS, AND W. R. PRYOR 1986. Photometry from Voyager 2: Initial results from the Uranian atmosphere, satellites and rings. *Science* **233**, 65–70.

LANE, A. L., R. A. WEST, C. W. HORD, R. M. NELSON, K. E. SIMMONS, W. R. PRYOR, L. W. ESPOSITO, L. J. HORN, B. D. WALLIS, B. J. BURATTI, T. G. BROPHY, P. YANAMANDRA-FISHER, J. E. COLWELL, D. A. BLISS, M. J. MAYO, AND W. D. SMYTHE 1989. Photometry from Voyager 2: Initial results from the Neptunian atmosphere, satellites and rings. *Science* **246**, 1450–1454.

LELLOUCH, E., W. B. HUBBARD, B. SICARDY, F. VILAS, AND P. BOUCHET 1986. Occultation determination of Neptune's oblateness and stratospheric methane mixing ratio. *Nature* **324**, 227–231.

MILLIS, R. L., L. H. WASSERMAN, AND P. BIRCH 1977. Detection of rings around Uranus. *Nature* **267**, 330–331.

MINK, D. G., AND A. KLEMOLA 1985. Predicted occultations by Uranus, Neptune and Pluto: 1985–1990. *Astron. J.* **90**, 1894–1899.

MINK, D. G., A. R. KLEMOLA, AND J. L. ELLIOT 1981. Predicted occultations by Neptune: 1981–1984. *Astron. J.* **86**, 135–140.

NARAYAN, R., AND W. B. HUBBARD 1988. Theory of anisotropic refractive scintillation: Application to stellar occultations by Neptune. *Astrophys. J.* **325**, 503–518.

NICHOLSON, P. D., M. L. COOKE, K. MATTHEWS, J. H. ELIAS, AND G. GILMORE 1990. Five stellar occultations by Neptune: Further observations of ring arcs *Icarus* **87**, 1–39.

NICHOLSON, P. D., B. A. MCLEOD, G. GILMORE, M. W. BUIE, AND K. MATTHEWS 1988. Near-infrared stellar occultation predictions for Uranus and Neptune: 1987–1990. *Astron. J.* **95**, 562–575.

OWEN, T., G. E. DANIELSON, A. F. COOK, C. HANSEN, V. L. HALL, AND T. C. DUXBURY 1979. Jupiter's rings. *Nature* **281**, 442–446.

REITSEMA, H. J., W. B. HUBBARD, L. A. LEBOFSKY, AND D. J. THOLEN 1982. Occultation by a possible third satellite of Neptune. *Science* **215**, 289–291.

ROQUES, F., M. MONCUQUET, AND B. SICARDY 1987. Stellar occultations by small bodies: Diffraction effects. *Astron. J.* **93**, 1549–1558.

ROQUES, F., B. SICARDY, P. BOUCHET, A. BRAHIC, R. HAFFNER, J. LECACHEUX, AND J. MANFROID 1984. Possible detection of a 10-kilometer object around Neptune. *Bull. Amer. Astron. Soc.* **16**, 1027–1028.

SICARDY, B. 1988. *Etude observationnelle, analytique et numérique des environnements planétaires. Applications aux anneaux de Saturne et d'Uranus et aux arcs de Neptune*. Thèse de Doctorat d'Etat, Université Paris 7.

SICARDY, B., P. BOUCHET, A. BRAHIC, R. A. MCLAREN, C. PERRIER,

AND F. ROQUES 1985. The 20 August 1985 stellar occultation by Neptune and its arc system. *Bull. Amer. Astron. Soc.* **17**, 923–924.

SICARDY, B., AND A. BRAHIC 1989. Search for dark matter around Neptune. *The Messenger—El Messagero* **56**, 41–45.

SICARDY, B., M. COMBES, A. BRAHIC, P. BOUCHET, C. PERRIER, AND R. COURTIN 1982. The 15 August 1980 occultation by the Uranian system: Structure of the rings and temperature of the upper atmosphere. *Icarus* **52**, 454–472.

SICARDY, B., F. ROQUES, A. BRAHIC, P. BOUCHET, J. P. MAILLARD, AND A. PERRIER 1986. More dark matter around Uranus and Neptune? *Nature* **320**, 729–731.

SMITH, B. A., L. A. SODERBLOM, D. BANFIELD, C. BARNET, A. T. BASILEVKSY, R. F. BEEBE, K. BOLLINGER, J. M. BOYCE, A. BRAHIC, G. A. BRIGGS, R. H. BROWN, C. CHYBA, S. A. COLLINS, T. COLVIN, A. F. COOK II, D. CRISP, S. K. CROFT, D. CRUIKSHANK, J. N. CUZZI, G. E. DANIELSON, M. E. DAVIES, E. DE JONG, L. DONES, D. GODFREY, J. GOGUEN, I. GRENIER, V. R. HAEMMERLE, H. HAMMEL, C. J. HANSEN, C. P. HELFEN-STEIN, C. HOWELL, G. E. HUNT, A. P. INGERSOLL, T. V. JOHNSON, J. KARGEL, R. KIRK, D. L. KUEHN, S. LIMAYE, H. MASURSKY, A. MCEWEN, D. MORRISON, T. OWEN, W. OWEN, J. B. POLLACK, C. C. PORCO, K. RAGES, P. ROGERS, D. RUDY, C. SAGAN, J. SCHWARTZ, E. M. SHOEMAKER, M. SHOWALTER, B. SICARDY, D. SIMONELLI, J. SPENCER, L. A. SROMOVSKY, C. STOKER, R. G. STROM, V. E. SUOMI, S. P. SYNOTT, R. J. TERRILE, P. THOMAS, W. R. THOMSON, A. VERBISCER, AND J. VEVERKA 1989. Voyager 2 at Neptune: Imaging science results. *Science* **246**, 1422–1449.

SMITH, B. A., L. A. SODERBLOM, R. F. BEEBE, J. BOYCE, G. A. BRIGGS, M. H. CARR, S. A. COLLINS, A. F. COOK II, G. E. DANIELSON, M. E. DAVIES, G. E. HUNT, A. P. INGERSOLL, T. V. JOHNSON, H. MASURSKY, J. F. MCCAULEY, D. MORRISON, T. OWEN, C. SAGAN, E. M. SHOEMAKER, R. G. STROM, V. E. SUOMI, AND J. VEVERKA 1979. The Galilean satellites and Jupiter: Voyager 2 imaging science results. *Science* **206**, 927–950.

SMITH, B. A., L. A. SODERBLOM, R. BEEBE, D. BLISS, J. M. BOYCE, A. BRAHIC, G. A. BRIGGS, R. H. BROWN, S. A. COLLINS, A. F. COOK, S. K. CROFT, J. N. CUZZI, G. E. DANIELSON, M. E. DAVIES, T. E. DOWLING, D. GODFREY, C. J. HANSEN, C. HARRIS, G. E. HUNT, A. P. INGERSOLL, T. V. JOHNSON, R. J. KRAUSS, H. MASURSKY, D. MORRISON, T. OWEN, J. B. PLESCIA, J. B. POLLACK, C. C. PORCO, K. RAGES, C. SAGAN, E. M. SHOEMAKER, L. A. SROMOVSKY, C. STOKER, R. G. STROM, V. E. SUOMI, S. P. SYNOTT, R. J. TERRILE, P. THOMAS, W. R. THOMPSON, AND J. VEVERKA 1986. Voyager 2 in the Uranian system: Imaging science results. *Science* **233**, 43–64.

TYLER, G. L., D. N. SWEETNAM, J. D. ANDERSON, J. K. CAMPBELL, V. R. ESHELMAN, D. P. HINSON, G. S. LEVY, E.A. MAROUF, AND R. A. SIMPSON 1986. Voyager 2 Radio Science observations of the Uranian System: Atmosphere, rings, and satellites. *Science* **233**, 79–84.

WALDROP, M. M. 1982. Neptune: a ring at last? *Science* **217**, 143.